Fatigue & Fracture behaviour of Zr-alloy processed through SPD

A Dissertation

Submitted in the partial fulfilment of the
requirement for the award of the degree
of

Master of Technology

In

Metallurgical and Materials Engineering

By

Vikas Agarwal
(14545013)

Department of Metallurgical and Materials Engineering

Indian Institute of Technology

Roorkee (India) – 247667

May, 2016

Candidate's Declaration

I hereby declare that the proposed work presented in this dissertation entitled **"Fatigue and Fracture behaviour of Zr-alloys processed through SPD"** in the partial fulfilment of the requirements for the award of the degree of Master of Technology in Material Science, submitted in the Metallurgical and Materials engineering department, Indian Institute of Technology Roorkee, is an authentic record of my own work carried out during the period from July 2015 to May 2016 under the supervision of **Dr. R Jayaganthan,** Professor Metallurgical and Materials engineering department and **Dr. G.P Chaudhary,** Associate Professor, Metallurgical and Materials engineering department, Indian Institute of Technology Roorkee, India.

The data presented in this dissertation has not been submitted by me for the award of any other degree.

Dated:

Place: IIT Roorkee **(Vikas Agarwal)**

This is to certify that the above statement made by the candidate is correct to the best of my knowledge and belief.

Dr R Jayaganthan

Professor

MMED

IIT Roorkee

Dr G. P Chaudhary

Associate Professor

MMED

IIT Roorkee

Acknowledgment

I take this opportunity to express with the utmost gratitude and sincere thanks to **Dr. R. Jayaganthan,** Professor, Metallurgical and Materials engineering department IIT Roorkee and Department of Engineering Design, IIT Madras and **Dr. G.P Chaudhary,** Associate Professor, Metallurgical and Materials engineering department, IIT Roorkee for their expert and kind guidance to my dissertation work. My work would have been directionless without their constant and patient guidance.

It is my pleasure to express my sincere gratitude to former and current Head of Department, Professors, Metallurgical and Materials Engineering Department, IIT Roorkee, **Dr. S. K. Nath** and **Dr. Anjan Sil** for providing me all the facilities required to carry out this work in the department.

I would like to extend my sincere gratitude to **Dr. D. Srivastava,** Head Physical Metallurgy Division, BARC**,** **Shri M. Kamesh,** Manager (BPS and BAR OP), NFC Hyderabad and **Shri S.K Jha** DGM (ISO, EX, BPS & BAR OP), Nuclear Fuel Complex (NFC), For allowing me to visit NFC Hyderabad and collect the samples for this project work. It is a pleasure for me to thank **Mr. Vishnu Narayan,** SO/C, NFC and **Mr. Chander Arora** SO/C NFC Hyderabad for their kind support throughout the project period**.**

I would like to thank **Dr. Sunkulp Goel, Mr. Nikhil Kumar, Ms. Devasri Flouria, Mr. Yogesha K. K., Mr. Amit Joshi, Mr. Raviraj Verma** and **Mr. Preet Yadav** for their co-operation and encouragement at every stage of this work.

I like to deeply thank some of my closest friends **Mr. Vignesh Srenivas**, **Mr. Gulshan Kumar Pradhan** and **Mr. Neeraj kumar Prasad** for their constant support and help.

I would like to thank all the **Technical Staff** at Metallurgical and Materials engineering department, IIT Roorkee and Indian Instrumentation Centre (IIC), IIT Roorkee, for helping me to access the labs and equipment. Last but not the least I would like to thank my family and friends for their constant moral support during the project work.

Date:

Place: IIT Roorkee **(Vikas Agarwal)**

Contents

List of Figures

List of Tables

Abstract

In Nuclear fuel complex, Hyderabad the bars of Zircaloy-4 (Zr-4) are used for the production of endcaps which is a critical component in terms of quality for Pressurised heavy water reactor (PHWR) fuel assembly. These endcaps are produced using cold swaging process. The cold swaging process comprises several steps for reduction in diameter of bars including several intermediate vacuum annealing process. These endcaps are used to seal the nuclear fuel rod from both the ends. Presence of even a minute crack will lead to leakage of radioactive substance into coolant during operation. In the present work a deep analysis has been carried out on microstructural and mechanical properties of Zircaloy 4 at each of these intermediate steps so that the gradual changes in the properties can be determined.

The Zircaloy-4 bar was subjected to cold swaging to reduce its cross section gradually from 23 mm diameter to 16 mm diameter via several passes of swaging followed by intermediate vacuum annealing at 732° for 3hr. Tensile test has shown increase in Tensile strength of the swaged sample with decrease in ductility. The dislocation density and fine grains formed during cold swaging impart improved yield strength to the deformed alloy. EBSD analysis helps to in understanding the grain orientation, size as well as twinning which helps in deformation. While TEM analysis was conducted to visualize the presence of dislocations density inside the material. Amount of dislocation density was determine using XRD and KAM studies. Corrosion test was conducted to determine the corrosion rate and it is found that the corrosion rate is decreasing with the intermediate steps and found to be least for the final product. Fracture analysis has been carried out on few samples to determine the fracture toughness at crack initiation and simulated fatigue results also indicates that the fatigue life is improving for the final product. All these results indicates that the process which is carried out to reduce the diameter of the rod via several swaging and annealing treatment helps in improving the desired properties of the material.

Chapter-1 Introduction

Zirconium alloys are extensively used in various types of fission reactors both light and heavy water types for different applications. It has HCP crystal structure and is highly used in nuclear industries due to their low neutron absorption coefficient and High temperature mechanical properties.[1][2] Zirconium alloys composed of 98-99% by weight zirconium, with the alloying elements like Iron, Chromium, Tin, Nickel.[3] Zirconium is currently used in the form of Zircaloy4, Zircaloy2, Zr-1Nb, Zr-2.5Nb and ZNC. Zr2 and Zr4 are used as fuel cladding tubes while Zr-2.5Nb and ZNC is used to make the pressure tubes and garter springs respectively.[4]

Zircaloy 4 which is uses to produce end caps of the nuclear fuel bundle are processed by the process called swaging. This is done to reduce the diameter of the rod in several steps. Zircaloy Ingots are coated with copper prior to the extrusion which acts as a lubricating agent. The 350mm dia. ingots are extruded to 152mm diameter billets. After extrusion the β quenching is performed. The billets are heated above the transformation temperature to about 1040^0C for around 30 minutes. At this temperature zirconium transforms to β phase and possess a BCC structure.[5] The alloying elements diffuse and a homogeneous material is produced. Following this the billet is rapidly quenched to α phase to prevent diffusion of alloying elements and thus the homogeneity is preserved. The quenched billet is then again hot extruded from 150mm to 23mm dia. bars. Further reduction in the diameter of the rods is done by the swaging process. The 23mm dia. bars are reduced to 16mm diameter by five pass swaging with two intermediate vacuum annealing treatments at 732° C for 3 hours. At 16mm swaged stage final annealing is done at same temperature and time.

Swaging is the process in which four radially moving anvils, or hammer dies are uses to produce solid or tubular component with constant varying cross section along their length.[6] These dies are mounted on a roller cage assembly which rotates and presses the die which in turn applies the compression force on the rod which is inserted for swaging. Due to the opposing motion of the hammers, no force is transmitted to the machine base. This process has several advantages like lower level of noise and vibration, uniform quality, no material loss, less heat generated, close tolerance and considerable savings in energy and material cost.[7]

Zirconium and its alloys are dominantly in α phase upto 850°C which has an HCP structure. The usual hexagonal cell can be seen as simple rhombohedral cell with two atom basis. The coordinate of the atoms can be written as (000) and (1/3, 2/3, 1/2). Essential plane in Zircaloy are the basal and the prism planes of the first and second order. Dominant mode of slip in Zr based alloys is the slip of dislocations on prismatic planes. In the alpha structure of Zircaloy slip takes place usually on the first order prism planes {10-10} along the <11-20> direction.[2] Slip has also been observed in the same direction on the basal plane but for a very low extend. In regions of high stress concentration such as grain boundaries slip occurs on {10-11} planes. Because of the limited number of the slip system in HCP structure Zircaloy undergoes substantial twinning during the plastic deformation. Under the tensile stress {10-12} <10-11> twins are activated and under compression {11-22} <11-23> twins are observed. Twinning does not allow high rates of deformation but it plays an important role in deformation by reorientation of the crystal in favourable slip system. Moreover it activates the new slip system even in the region of local stress concentration such as twin boundaries or by interaction between dislocation and twinning.[8]

Zircaloy 4 are uses to produce end caps of the nuclear fuel bundle are produced by the swaging process. 23 mm diameter extruded rod is converted to 16 mm diameter rod in several steps. This present study involves understanding the changes that are taking place in the several steps of the swaging process and also to understand the effect of swaging on Zircaloy4 by determining several properties of the material like tensile, hardness, corrosion resistance, and fracture toughness and by characterizing technique like EBSD and TEM. X-ray studies have also been carried out to calculate the dislocation density in the material by Williamson Hall method.[9] Strain rate sensitivity index (m) is determined by doing tensile test at different strain rate to understand the flow behaviour of the material.[10]

Chapter-2 Literature Survey

2.1 Zirconium and its alloys

Zirconium is a chemical element having atomic number 40. It is extracted from the mineral known as Zircon. It has an HCP structure (α phase) below 865° C and a BCC structure (β phase) above 865°C, its melting point is 1855°C.[11] Zirconium is highly used in nuclear industries due to its low neutron absorption coefficient. However pure Zr does not possess good strength at high temperature so alloying is done to improve high temperature strength. Corrosion strength is affected by presence of the impurities.[12] So to impart good strength at high temperature and to improve corrosion resistance various alloys has been made and widely used.

Zirconium alloys composed of 98-99% zirconium (by Weight percent), with the alloying elements being tin, iron, chromium and nickel. Currently zirconium is used in the form of Zircaloy-2(Zr2), Zircaloy-4(Zr4), Zr-1%Nb and Zr-2.5%Nb. Zr2 and Zr4 are generally use for fuel cladding rods in nuclear fuel reactors. Zr4 is Ni free form of Zr2. Its corrosion resistance is same as Zr2 while its hydrogen absorption tendency reduces to half.[11] Hydrogen is a major impurity element in zirconium alloys which forms hydrides. The composition of Zircaloy-4 is given in table1.

Table 1 composition of Zircaloy 4 in weight percent.

Element	Zirconium	Tin	Iron	Chromium	Oxygen	Permitted Impurities
Wt%	>95%	1.2-1.7	0.18-0.24	0.07-.13	900-1400 ppm	Balance

2.1.1 Importance of Zircaloy4

Zircaloy-4 is widely used in the manufacturing of bars, tubes, sheets and wires for fabrication of various products such as end caps, end plugs, fuel tube, bearing pad, spacer pad, end plate and garter springs and various assemblies and subassemblies of reactor due to its low neutron absorption cross section, high corrosion resistance and high temperature strength. The sheets are used to produce endplates, spacer pads for PHWR fuel assembly. End plates are required to keep the fuel element in contact using resistance welding techniques. Spacer pads are used in assembly for spacing between fuel elements to effectively remove heat. The wires are used to produce garter spring, girdle wire and breaking pads.

Swaged Zr4 bars are uses to produce end caps of a nuclear fuel bundle and end plugs for BWR and PWR. These end caps are one of the most critical components in fuel assembly as these are welded to fuel tubes loaded with uranium pellets for containment.[11][13] A defect of 2-3 micro meters can result into leakage of radioactive substance into the reactor. To prevent the failure in the reactor end caps are required to be defect free and meet standard stringent quality criteria.

2.2 Swaging

Swaging or radial forging is generally a cold forging process which utilizes two or more radially moving dies for production of solid or tubular components with constant varying cross sections along their length.[14] In this process diameter of the rods are reduces while their length increases because no restriction is provided in vertical direction. If a hollow shape is required and a mandrel is generally used. Below figure shows the scheme of rotary forging or swaging.

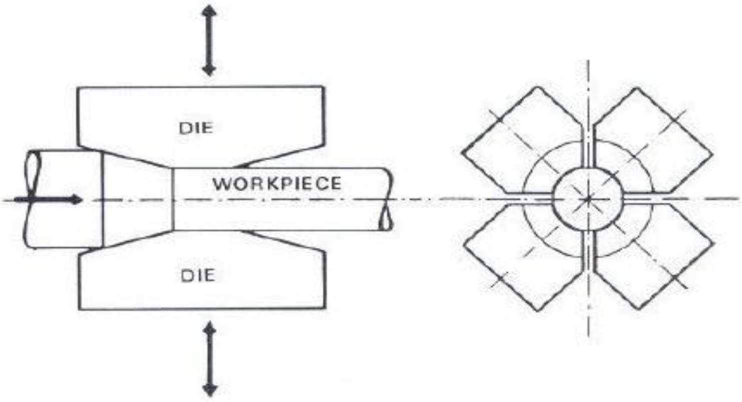

Figure 1 schematic representation of swaging die and work piece.

Deformation in the radial forging process results from a large number of short-stoke side pressing around the work piece. A typical hammer type arrangement is shown in above figure. The forging actions of the radial forge takes place within a vertically arranged forging box containing the four hammers and two drives located at the right angle to one another. Due to opposing motion of the hammers there is no force which is transmitted to the machine base.

In swaging process there exist three deformation zones exits. The name of these zones are sinking, forging and sizing. Sinking is the first zone of deformation in which material enters into the dies. In some cases this zone is very small like during finish forging of the tube.

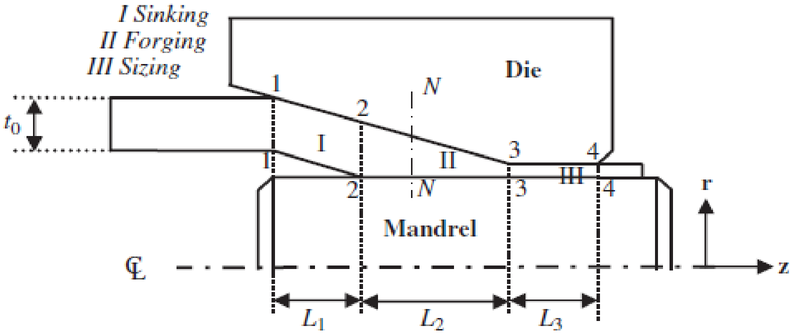

Figure 2 Zones involved in swaging process

The deforming material may either flow relatively towards the product or towards the perform or in both of these direction. This flow depends on the inlet cone angle α. Thus in general a neutral plane (N-N) does exist and at this plane he material does not flow axially it only deforms radially.[6][15][16][17]

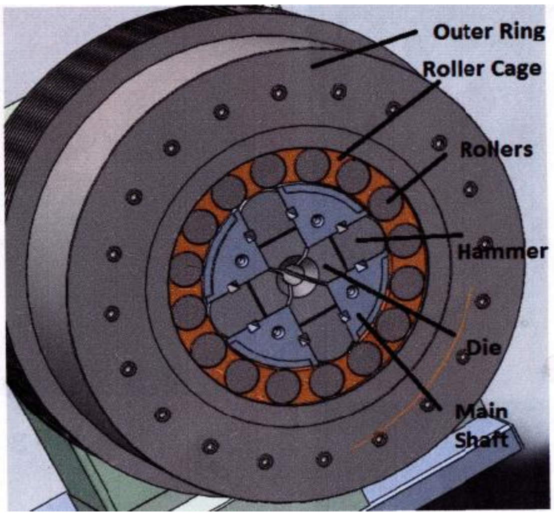

Figure 3 schematic of die and roller assembly

The total work that is required during swaging process can be divided into three components. The first component is the plastic work or the strain energy, the second one is the frictional work and the last one is the shear work which is dissipated when the material flow direction is changed.

For the swaging of the rods and tubes, several types of die configuration are available. For the swaging of round bars or tubes, round dies or flat-faced dies can be used. Round dies are particularly suitable for the bar stock, since these dies do not necessary require the billet to be of round cross-section. The universal die is situated for swaging round as well as square and rectangular cross sections.

2.3 Deformation mechanism in Zircaloy-4

2.3.1 Slip system in Zr4

At temperature below 850° C, Zirconium has an HCP crystal structure with c/a ratio less than 1.633. The usual hexagonal cell can be seen as a simple rhombohedral cell with a two atom basis. The coordinates of the atoms are (0,0,0) and (1/3,2/3,1/2).[4][18][19] Essential planes in the hcp system are the basal plane and prism planes of the first and second order. Basal and prism planes are perpendicular to each other and have an <a> direction as the common lattice vector. The planes oriented in between are pyramidal plane of different type and order.[20][2]

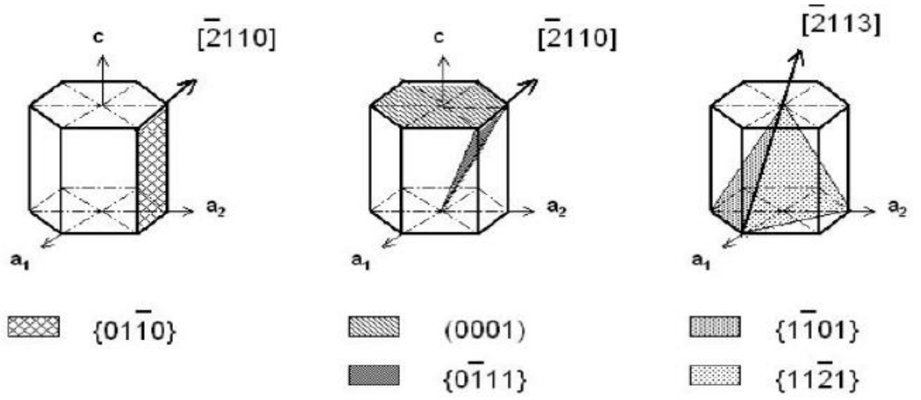

Figure 4 slip system in swaging process

Besides the factor like stacking fault energy and the dependence of the crystal orientation, the c/a has a dominant influence on the deformation system to be activated. According to the Peierls-Nabarro model, one can expects that the basal slip will be replace by prism slip as soon as c/a ratio becomes less than 1.732. In this case the inter planer spacing of the prism planes and their atomic packing density becomes larger than the corresponding values for the basal plane. This is the reason why the dominant mode of slip in Zirconium alloys is the slip of dislocation on prismatic planes i.e. {10-10} planes along the <1-210> direction. It has been reported that during cold working process like swaging prismatic slip becomes harder and thus making twinning to get activated. A slip system with a component in the <c> direction has been observed only under constraints and at high deformation temperature. The corresponding slip mode is slip that occurs on first or second order pyramidal planes {10-11} or {1-211} in <11-23> direction.

2.3.2 Twinning in Zr4

Because of the limited number of slip system available Zr undergoes substantial twinning during plastic deformation. Under tensile stress {10-12} <10-11> twins are activated and less commonly {11-21} <11-26> twins. Under compression {11-22} <11-23> and at elevated temperature {10-11} <10-12> twinning is observed. Twinning does not allow high rates deformation; however it plays an important role in deformation by reorienting the crystal to favourable slip system and thus allowing the possibility of larger strains. Moreover twinning activates new slip system even in the region of local stress concentration, such as twin boundaries or by interaction between dislocation and twinning.[21]

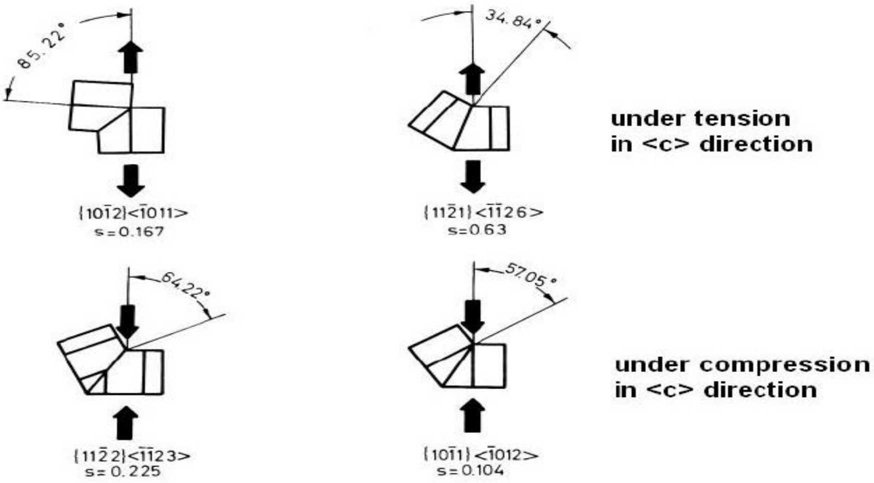

Figure 5 Types of twinning involved in Zirconium alloys

Yong Choi [22] has studied about the texture development of zirconium alloy processed by pilgering and its effect on corrosion behavior, In that study he found that grain size of the alloy is decreasing with the pilgering process and corrosion rate is increasing because of it. He also reported that crystallographic texture influences the corrosion rate of the Zircaloy.

Chapter 3- Experimental Procedure

3.1 Swaging

Swaging is cold rotary forging process in which four radially moving anvils produces solid or tubular component with constant varying cross section. This process is generally used to reduce the diameter of the bars. To produce the end caps of nuclear fuel bundle 23 mm dia. Extruded rod is swaged to 16mm diameter rod in 5 pass swaging with 2 intermediate annealing at 732°C for 3 hours and a final annealing (same time and temperature) after 16mm diameter swaging. Figure 6 shows the swaging machine available at NFC, Hyderabad. This machine is use to produce end caps of nuclear fuel bundle. The rod is placed in the holder which not only holds the rod but also reduces the vibrations. Holder presses the rod inside the machine and the die-roller assembly compresses the rod which in turn reduces its diameter by increasing in length. The strain is around 15-20% in each step, low strain is given to prevent the grain growth in annealing process.

Figure 6 Rotary swaging machine at nuclear fuel complex, Hyderabad.

3.2 Optical Microscopy

Microstructure of Zr4 samples has been obtained by using LECIA DMI5000 M optical microscope. All the samples were polished using emery paper upto 2000 grit size followed by cloth polishing using alumina powder. Then etching of the samples was done by 10:45:45 ratio of HF, HNO_3 and distilled water respectively for 5-10 seconds. The optical imaged after etching was not clear so electro-polishing was also done using 20:80 ratio perchloric acid and methanol at 30V and -40°C temperature.

Figure 7 LECIA DMI5000M optical microscope

3.3 Tensile Test

Tensile test of all the Zircaloy 4 samples were carried out using S-Series H25K-S tensile testing machine with the cross head speed of 1mm per minute. The sample for the test was prepared as per ASTM E8 [23]substandard size specimen of gauge length 30mm and diameter 6mm. Three samples were tested in each condition and average of all the three was considered.

Figure 8 H25K-S tensile testing machine

To determine the strain rate sensitivity of the material four conditions out of seven is chosen i.e. from 21mm swaged to 19mm Annealed and tensile test is carried out at different strain rates.

3.4 Micro hardness test

UHL VHMT micro hardness testing machine was used with 500gf load with indentation speed of 50 µm/sec at room temperature for measuring micro hardness of all the samples. Minimum of 5 readings were taken for the hardness and the average value was considered. Surface of the sample was initially polished up to a 2000 grit size emery paper followed by cloth polishing using 0.05µm grain size alumina powder.

Figure 9 Micro hardness Testing setup

3.5 X-ray diffraction (XRD)

All the samples were characterized by using XRD (Bruker AXS D8 Advance instrument) with Cu Kα radiation from 20 to 120 degree angle at a scan rate of 1 degree per minute. Expert high score plus (2.2.5) software is used to identify the formation of different phases in the sample using XRD data.

It is assumed that the peak broadening takes place because of the size effect and the strain effect. The sub grain size (D) and the micro strain $<\varepsilon^2>^{1/2}$ were calculated from the integral breadth of XRD peak by applying “Williamson-Hall” Technique and the dislocation density was estimated using formula [24].

$$\rho = \frac{2\sqrt{3}}{Db} < \varepsilon^2 >^{1/2} \text{………………………}(1)$$

Where b is burger vector of the HCP crystal, D is sub grain size, ρ is the dislocation density.

3.6 Three point bend test

Three point bend test is also carried out using S-Series H25K-S universal testing machine. This test is use to determine the Fracture toughness values of the samples. Fracture toughness evaluation was carried out with crosshead speed of 5mm/min on chevron notch 3 point bend specimen as shown in Figure 10. The 3 point bend specimen prepared was having span length (L) of 68 mm, thickness (B) of 7.5 mm and a width (W) of 15 mm. The depth of notch and pre crack (a) was 7.5 mm, the ratio of a/w maintained less than 0.55. Generally, fracture toughness is assessed using J-Integral measurements by applying a multiple specimen test procedure. In this experiment fracture energy is calculated as per ASTM 1820E basic test method. At least 3 test samples were tested from every processing condition for required accuracy.

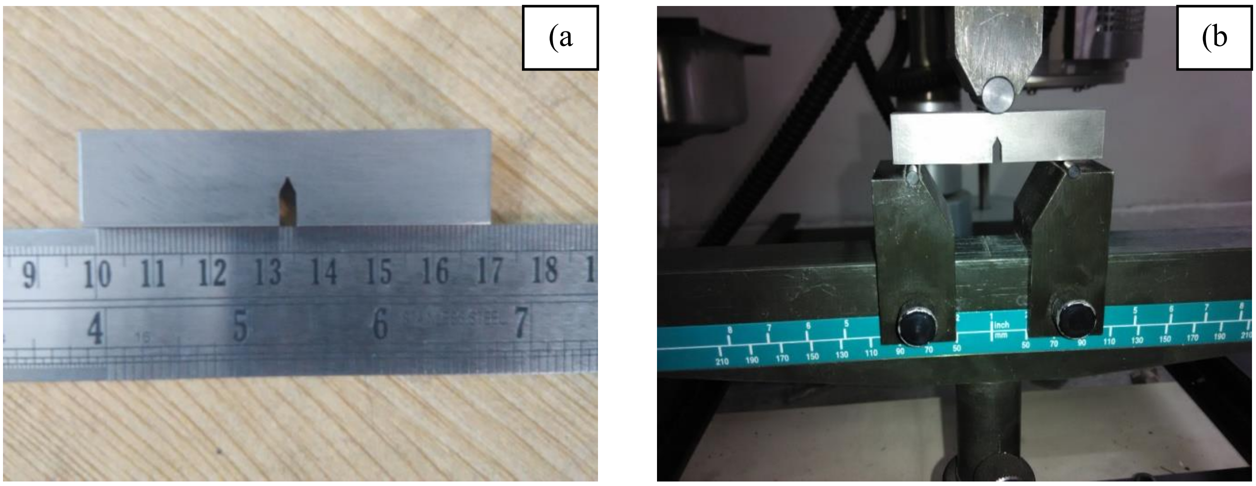

Figure 10 (a) Three point bend test specimen (b) Setup for Three point bend test

3.7 Transmission electron Microscopy (TEM)

Transmission electron microscopy was done using Tecnai G2 20 machine. For this test all the samples were thinned upto 0.1 mm thickness using emery paper of grit size 320-2000 washed into acetone and then punched to 3mm diameter disc. These discs then further polished by using twin jet polishing machine in which 20:80 ratio perchloric acid and methanol was used as an etchant. The voltage and the temperature were 30 V and -400C respectively.

Figure 11 Tecnai G2 20 Transmission electron microscopy machine

3.7 Scanning Electron microscopy (SEM)

The Carl Zeiss EVO18® SEM with LaB6 filament was used for the Fractography of the fractured tensile test samples and for EBSD analysis. The fracture surface of tensile test samples of different condition processed samples was examined using SEM. Any sample preparation is not necessary for Fractography analysis. SEM is also used for EBSD analysis of Zr4 samples. All the samples were polished using emery paper from 320 grit sizes to 2000 grit size followed by cloth polishing with alumina powder. Then etching of the sample was done by 10:45:45 ratio of HF, HNO3 and distilled water respectively. Electro polishing of the samples then were done using 20:80 ratio perchloric acid and methanol as of TEM sample preparation was used and at a voltage of 20V and -30°C Temperature.

Figure 12 Carl Zeiss EVO18® SEM machine

3.8 Corrosion Test

Grammy potentiostat (interface 1000) was use for the polarization curve (Tafel Curve). The setup includes three electrodes i.e. working electrode (sample), Reference electrode (saturated calomel electrode) and counter electrode (platinum). An area of 0.785 cm^2 has been exposed in the corrosive environment (1 M NaCl solution).

The polarization test has been performed on the samples at a scan rate of 1mV/s. corrosion rate in mm per year is determined using the formula [25]

$CR = 3.27 * 10^{-3} \ \frac{EW * i_{corr}}{\rho}$ …………………… (2)

Where EW is equivalent weight and ρ is the density of the material.

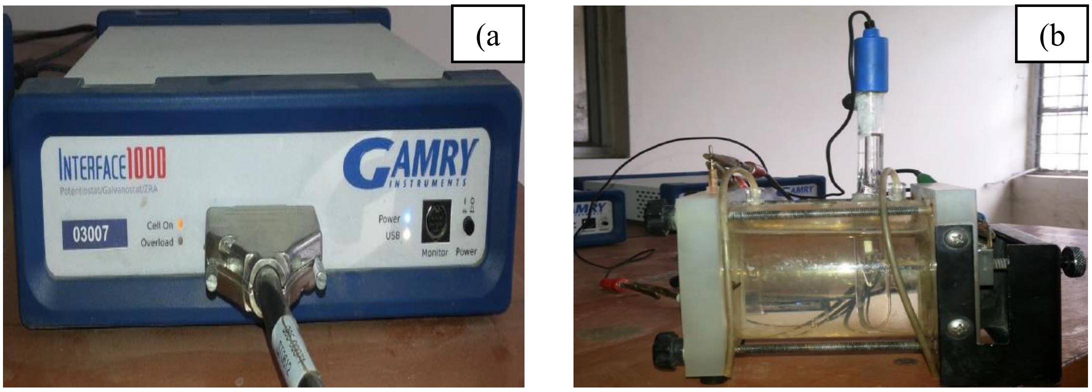

Figure 13 (a) Gamry interface 1000 (b) Electrochemical cell with three electrodes

Chapter 4 - Results and Discussion

Zircaloy 4 which is use to make end caps for nuclear fuel bundle are produce by the swaging process in several stages. First the 350 mm diameter Zirconium ingot is extruded to 152mm diameter billets. This extrusion is done at 850° C using copper at the surface which acts as lubricating agent for the extrusion process. After this the billet is heated to 1040°C where Zr transforms to β-phase and possess a BCC structure. The alloying elements diffuse and a homogeneous material is produced. Following this the billet is rapidly quenched to α-phase to prevent diffusion of alloying element and thus homogeneity is preserved. The quenched billet is again hot extruded from 150mm to 23mm bars. After this 23mm extruded rods is converted into 21 mm swaged rod using rotary swaging machine in two pass followed by intermediate annealing at 732°C for 3 hours. 21 mm annealed rod is then converted into 19 mm swaged rod in single pass swaging followed by vacuum annealing for same time and temperature. 19 mm annealed rod is then finally swaged to 16 mm swaged rod in two pass swaging. The rod is then send for final annealing treatment and after series of test and straightening process machining of the rod is carried out to form the end caps. Below is the flow chart of the step wise swaging process, it is also indicating the stages from where samples have been collected for the analysis.

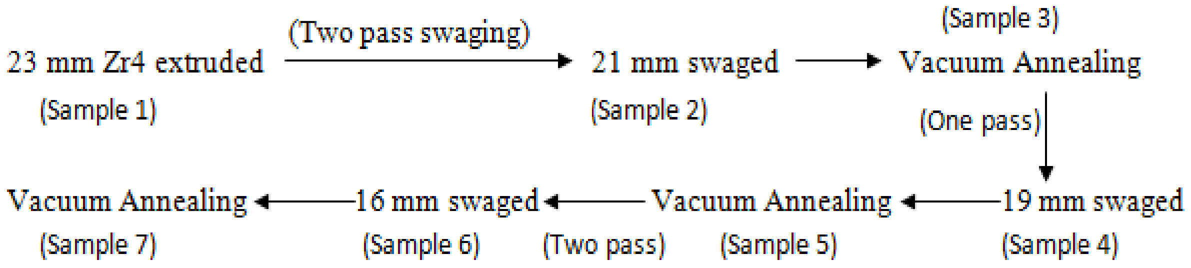

Figure 14 Different swaging steps for the production of end caps at nuclear fuel complex, Hyderabad

All the seven conditions rods i.e. 23 extruded, 21 swaged, 21 annealed, 19 swaged, 19 annealed, 16 swaged and 16 annealed were cut along the cross section for the characterization purposes like optical microscopy, EBSD, TEM etc. Tensile samples were also prepared along the longitudinal direction of the rod.

4.1 Optical Microscopy

Figure 15 shows the optical microscopy images of the Zircaloy 4 samples at different swaging and annealing condition. All the swaged samples i.e. figure 15(b, d, f) shows deformed grains, the grains are compressed and slightly elliptical due to the swaging process. While all the annealed sample shows homogeneous and Equiaxed grains. The grain size is determine using linear intercept method.

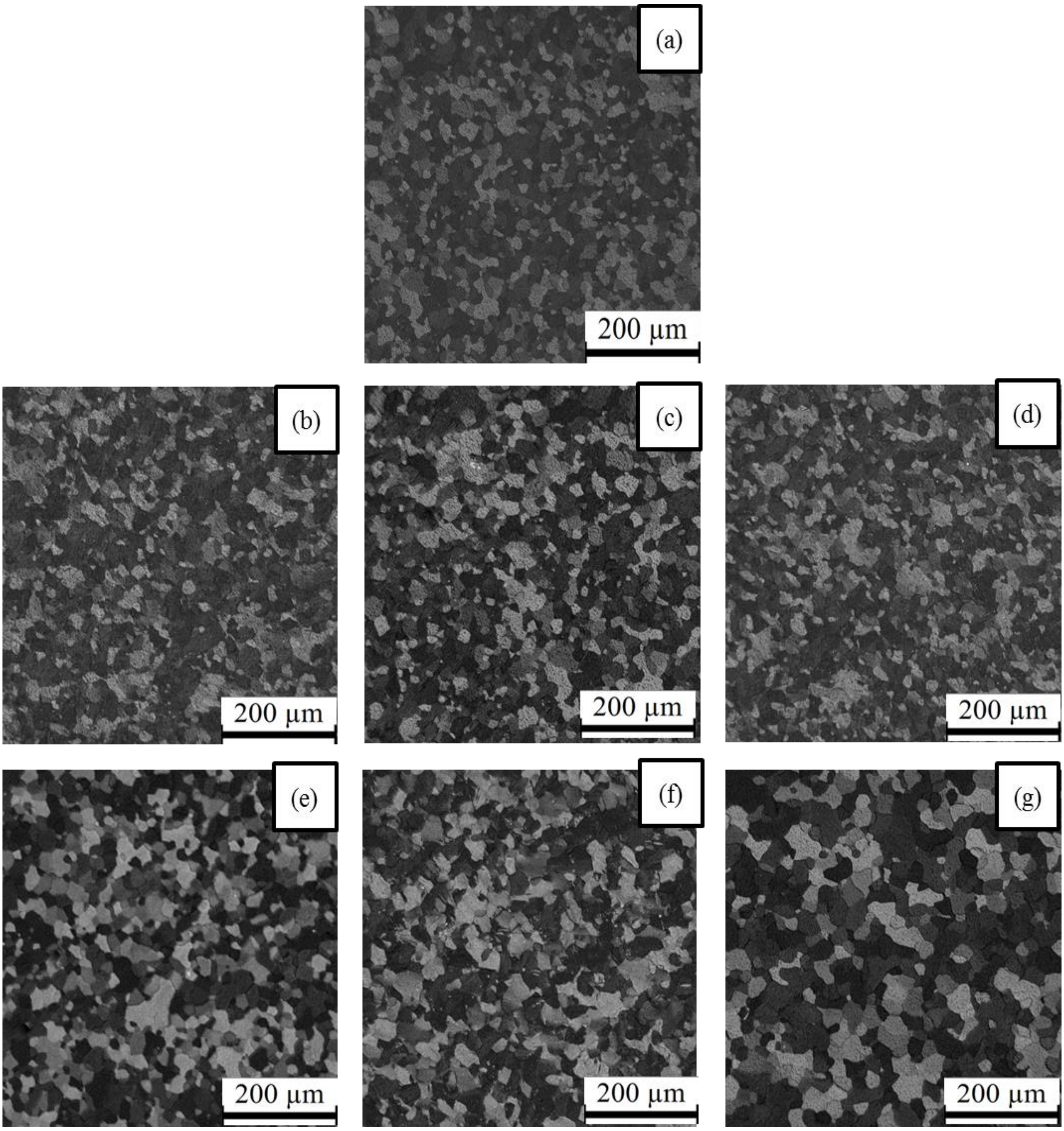

Figure 15 Optical micrograph of a) 23 extruded b) 21 swaged c) 21 Annealed d) 19 swaged e) 19 Annealed f)16 Swaged g) 16 annealed Zr4 samples

The swaged rods has refined grains on the cross section surface. Initially the grain size was around 8 µm of 23mm extruded sample. It decreases to 6 µm for 21 swaged sample. This means in a 12% reduction process the grain size decreases to 25%. After the first intermediate annealing treatment the grain size becomes 17 µm. After further reduction of 21mm annealed rod to 19 mm swaged rod the grain size decreases to 14 µm. This means a single step of 9.5% reduction reduces the grain size by 17.6 %. After annealing this 19 mm swaged sample the grain size increases to 22 µm. Further reduction of the rod to 16 mm i.e. a stain of 15.7% reduces the grain size to 16 µm i.e. percentage grain size reduction of 27.27%. And finally the 16mm annealed sample has a grain size of around 24 µm, below is the table shows the grain sizes at different steps.

Table 2 Grain sizes of different samples determined by linear intercept method

Samples	23 extruded	21 swaged	21 annealed	19 swaged	19 annealed	16 swaged	16 annealed
Grain size by linear intercept method	8 µm	6 µm	17 µm	14 µm	22 µm	16 µm	24 µm

4.2 Tensile and Micro hardness test.

Engineering stress- strain curve is shown in figure 16 (a) for all the Zr4 samples under uniaxial tensile loading with strain rate of $5.55*10^{-4}$ per sec. Tensile stress is increases from 570Mpa to 637MPa after first pass of swaging process i.e. from 23 mm extruded to 21 swaged, with decrease in percentage elongation from 27.93% to 12.6%. After the intermediate vacuum annealing the tensile stress decrease to 474MPa with the improvement in the ductility. This fall and rise of the tensile strength takes place during the processing stages but an interesting trend has been observed here. The tensile stress is decreases after each swaging step compared to its previous step while it increases after each vacuum annealing treatment compared to its previous stage as shown in figure 4.3(b). Like tensile stress of 21 swaged sample was 637MPa it decrease to 605MPa in 19 swaged sample and then finally to 589Mpa in 16 swaged sample while if we see this trend in annealing stage then it was 474MPa in 21 Annealed stage increases to 485Mpa in 19 annealed stage and then finally it becomes 491Mpa in 16 Annealed stage. The reason for this decrease in tensile stress is assume to be increase in grain size which is given by Hall-Petch relationship. As the grain size is increasing from 21mm swaged to 16mm swaged the tensile stress is decreasing. There is as slight increase in tensile strength from 21 annealed to 16 annealed sample although their grain size is also increasing. The reason for this increase in tensile stress is assume to be increase in dislocation density inside the material. This is further validated by dislocation density measurement by Williamson hall method using XRD. [24]

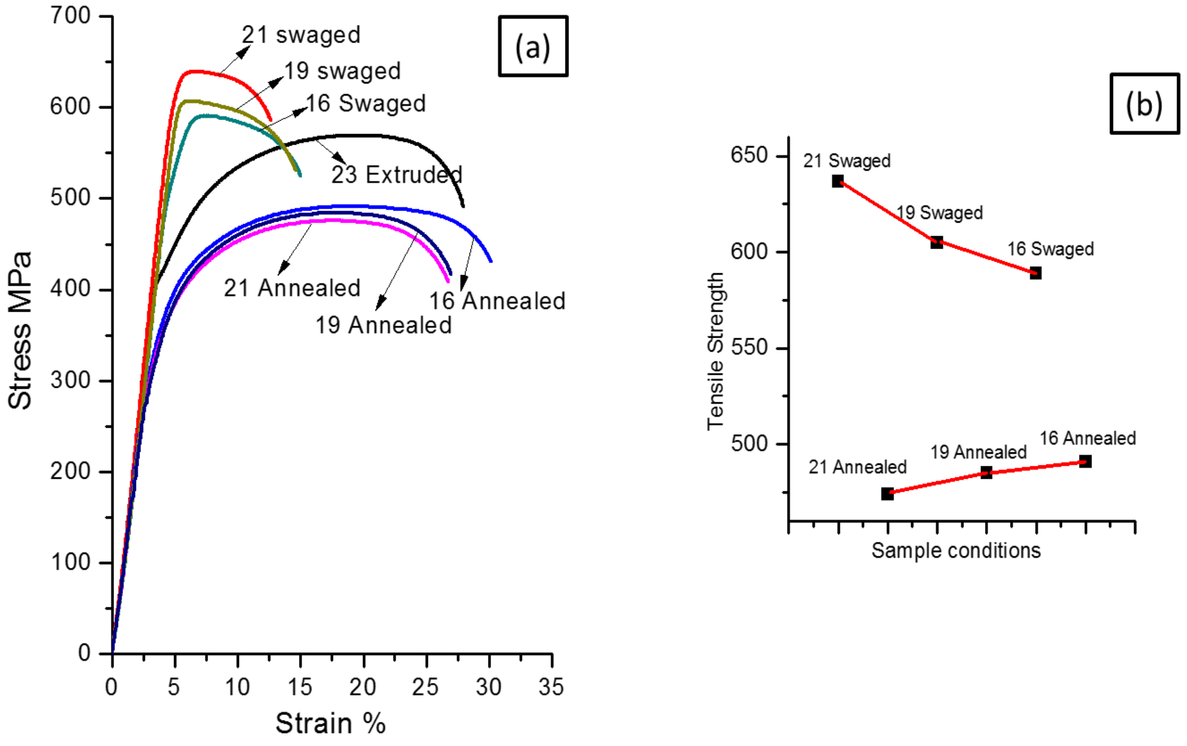

Figure 16 a) Engineering stress-strain curve of Zr4 samples and b) Variation of tensile stress at different conditions

The hardness of the Zr4 samples almost follow the same trend as it was following for tensile strength, it increases from 181Hv in 23mm extruded sample to 200Hv in 21 Swaged and then decreases to 170Hv in 21 Annealed. The hardness also decreases as compared to its previous swaged step and increases as compared to its previous annealed step i.e. it increases from 170Hv in 21 Annealed to 178Hv in 19 Annealed and the finally to 183.5Hv in 16 Annealed stage.

Table 3 values of yield stress, tensile stress and micro hardness of Zr4 samples at different conditions

Samples	23 extruded	21 swaged	21 annealed	19 swaged	19 annealed	16 swaged	16 annealed
MicroHardness (Hv)	181	200	170	198	178	194	183.5
Y.S (MPa)	416	633	384	601	387	587	383
T.S (MPa)	540	639	474	605	485	589	491

The variation of hardness at different swaging and annealing steps is shown below. Also table 3 shows the values of yields stress, tensile stress and micro hardness of Zr4 samples at different processing stages.

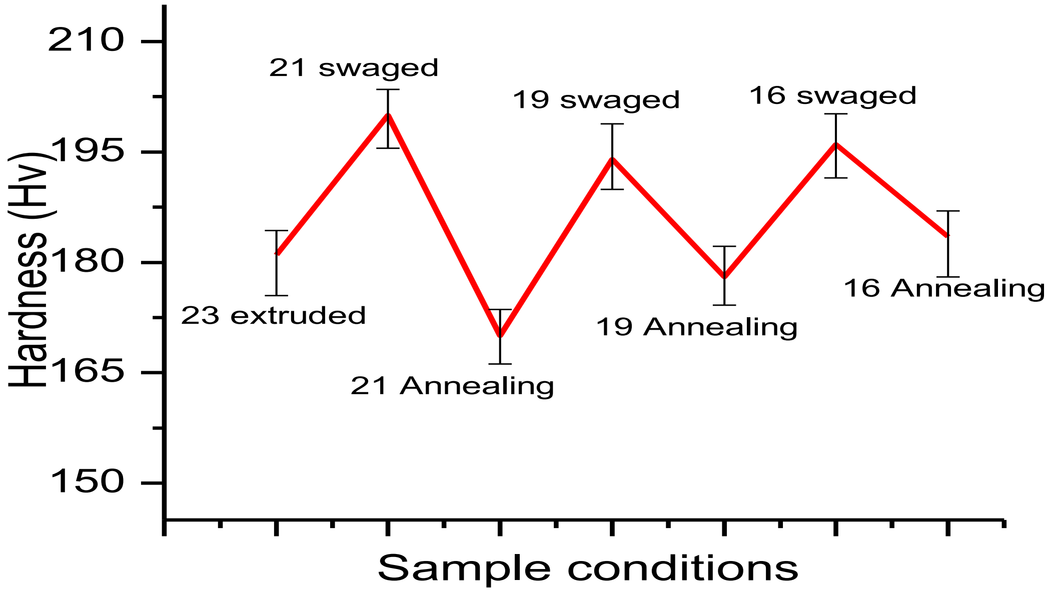

Figure 17 Change in hardness with swaging and annealing process of Zr4 samples

Tensile test at different strain rates has also been done to determine the strain rate sensitivity of the material. In the present work four stages from the above seven stage has been chosen (from 21 swaged to 19 Annealed) and tensile test is carried out at strain rates of $2.2*10^{-3}$, $3.33*10^{-3}$, $4.45*10^{-3}$ and $5.55*10^{-3}$ per second at room temperature as shown in Figure 18. The rate at which strain is applied to a specimen can have an important influence on the flow stress. Increasing in the strain rate increases the flow stress. A general relationship between flow stress and strain rate at constant strain and temperature is given as [26]

$$\sigma_t = C(\dot{\epsilon})^m|_{\epsilon,T} \text{ ……………………. (3)}$$

Where m is known as strain rate sensitivity or strain rate sensitivity index, $\dot{\epsilon}$ is strain rate per second and C is empirical constant. This index m can be obtained by the slope of the plot of log$\boldsymbol{\sigma}$ vs. log$\dot{\epsilon}$, where $\boldsymbol{\sigma}$ is the true yield stress or for small strain rate values it is advisable to use the formula[10][26] $m = \frac{ln(\sigma_t^2/\sigma_t^1)}{ln(\dot{\varepsilon}_2/\dot{\varepsilon}_1)}$ …….. (4) Because in this case the tilt of stress strain curves has a maximum value.

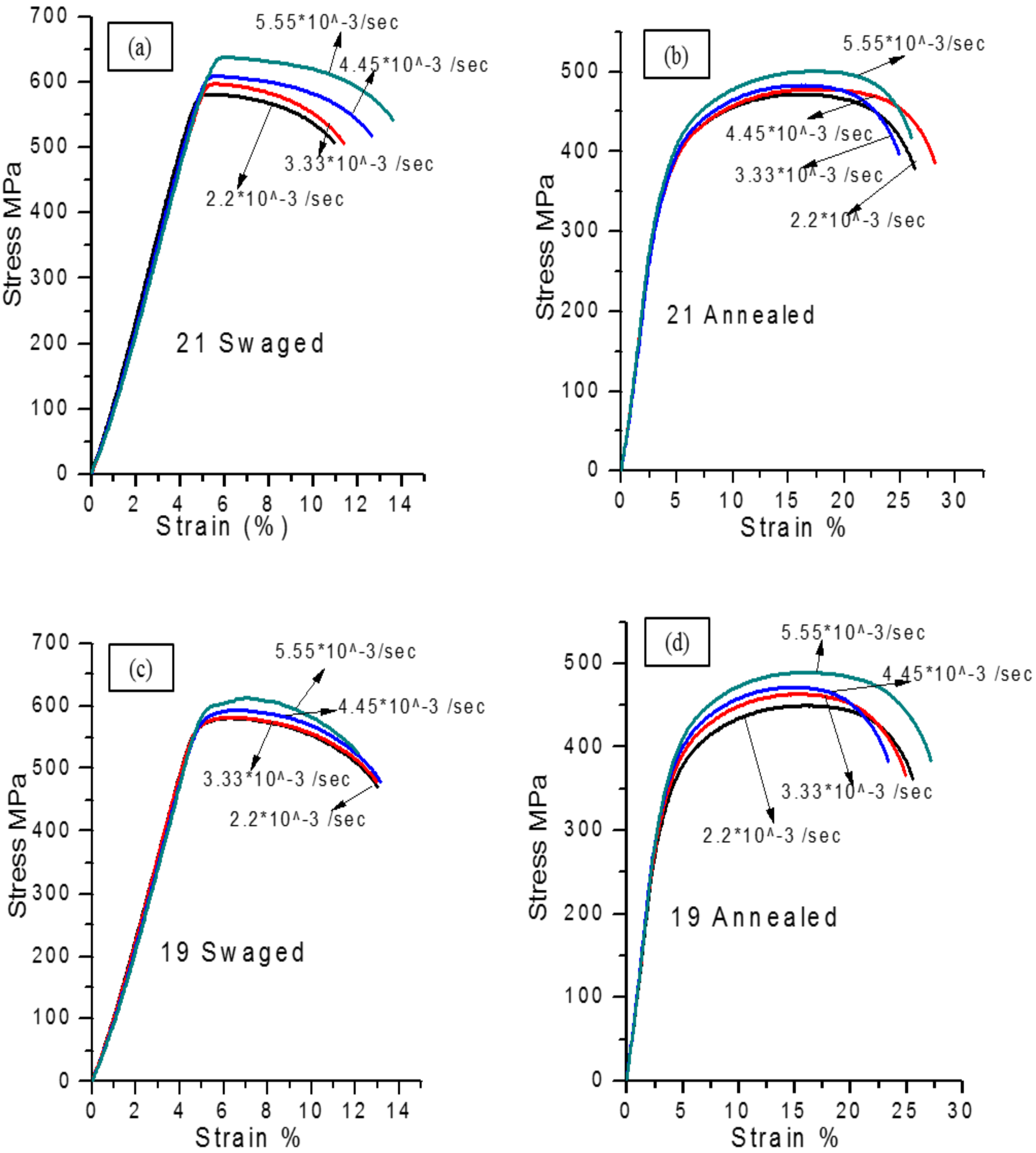

Figure 18 Engineering stress strain curve at different strain rate of (a) 21 swaged, (b) 21 Annealed, (c) 19 swaged and (e) 19 annealed Zr4 samples

Values of strain rate sensitivity index determines using above equation form “m” is given below in table 4

Table 4 values of strain rate sensitivity index of Zr4 samples at different conditions

Samples	21 swaged	21 annealed	19 swaged	19 annealed
Strain rate senstivity index (m)	0.129	0.0708	0.0652	0.0623

Strain rate sensitivity is a good indicator of changes in deformation behaviour and measurement of m provides a key link between dislocation concepts of plastic deformation and the more macroscopic measurements made in tension test. The strain rate sensitivity index is found to decrease continuously from 0.129 for 21 swaged to 0.0708 for 21 Annealed and from 0.0652 for 19 swaged to 0.0623 for 19 swaged. The reason for this decrease in sensitivity is assumed to be due to increase in the grain size of the material.

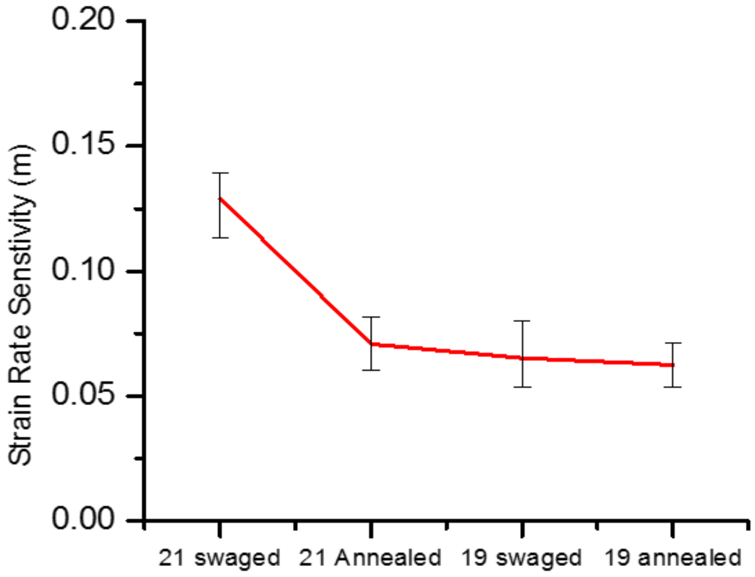

Figure 19 variation of strain rate sensitivity of Zr4 samples at different swaging and annealing steps.

4.3 Fractography Analysis

The fractured surface is examined under scanning electron microscope to analyse the kind of fracture that takes place after tensile test for strain rate of $5.55*10^{-4}$ per sec. Fractography images is shown in figure 20 at a magnification of 3000X. The micrograph obtain reveals that the nature of the fracture was inter granular. The dimple size of the 23mm extruded and 21 mm swaged sample is small as compared to other condition which corresponds to its grain size as the grain size of 23 mm extruded and 21 mm swaged sample was 8 and 6 µm respectively.

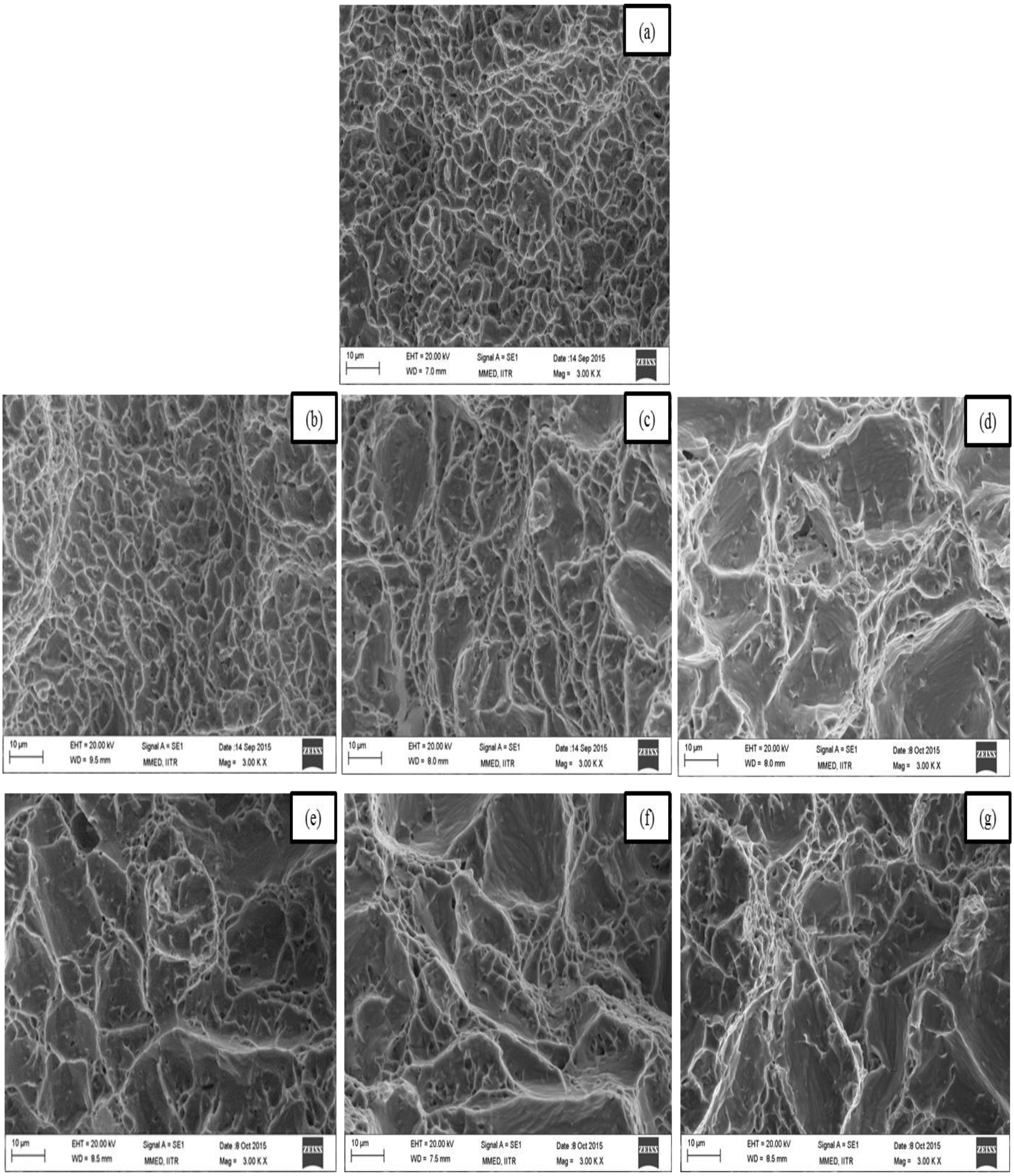

Figure 20 Fractography images of a) 23 extruded b) 21 swaged c) 21 Annealed d) 19 swaged e) 19 Annealed f)16 Swaged g) 16 annealed Zr4 samples

The crystallographic mode of fracture in 23mm extruded and 21 mm swaged samples was cleavage because cleavage fracture appears bright and granular which is clearly visible in figure

20(a, b). In case of 19 mm and 16 mm swaged Zr4 samples i.e. from figure 20(d, f) few facets were observed at some location and fine dimples at other. This suggest that the nature of fracture in these samples were mix mode (partly ductile and partly brittle). In case of annealed samples the fracture was along the grain boundaries and the degree of ductility is increasing from 21 mm annealed to 16 mm annealed sample as more number of fibres are clearly visible.

The Fractography analysis after tensile test at different strain rate is also done to determine the effect of strain rate on the mode of fracture. This is shown in figure from 21 to 24.

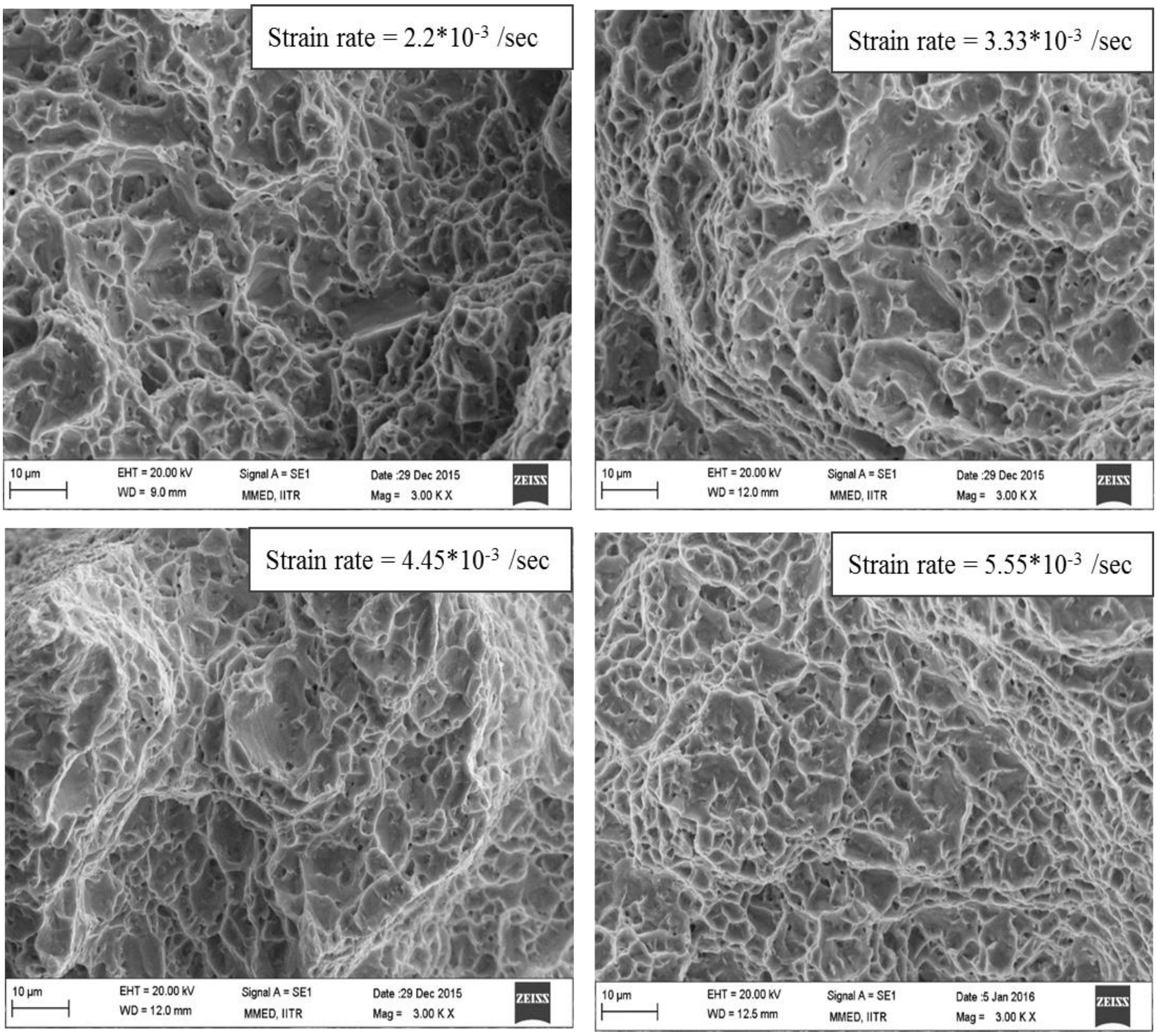

Figure 21 SEM micrograph of the fractured surface of 21mm swaged sample at different strain rate

The Fractography images of 21mm swaged sample at different strain rate as shown in figure 21 reveals the fracture is mostly intergranular. The dimple size is found to be decreasing slightly as the strain rate is increasing. In case of 21 mm annealed sample small amount of tearing is observed also as the strain rate is increasing the density of dimples is decreasing which is the attribute of brittle fracture. In case of 19 mm swaged samples (figure 23) the amount of ductile fracture is decreasing as the strain rate is increasing which is depicted by the presence of facets and small dimples. Also in case of 19 mm annealed samples (figure 24) as the strain rate is increasing the presence of facets and tear band is increasing. Thus it can be depicted as we increase the cross head velocity in normal tensile test the percentage of ductile fracture decreases.

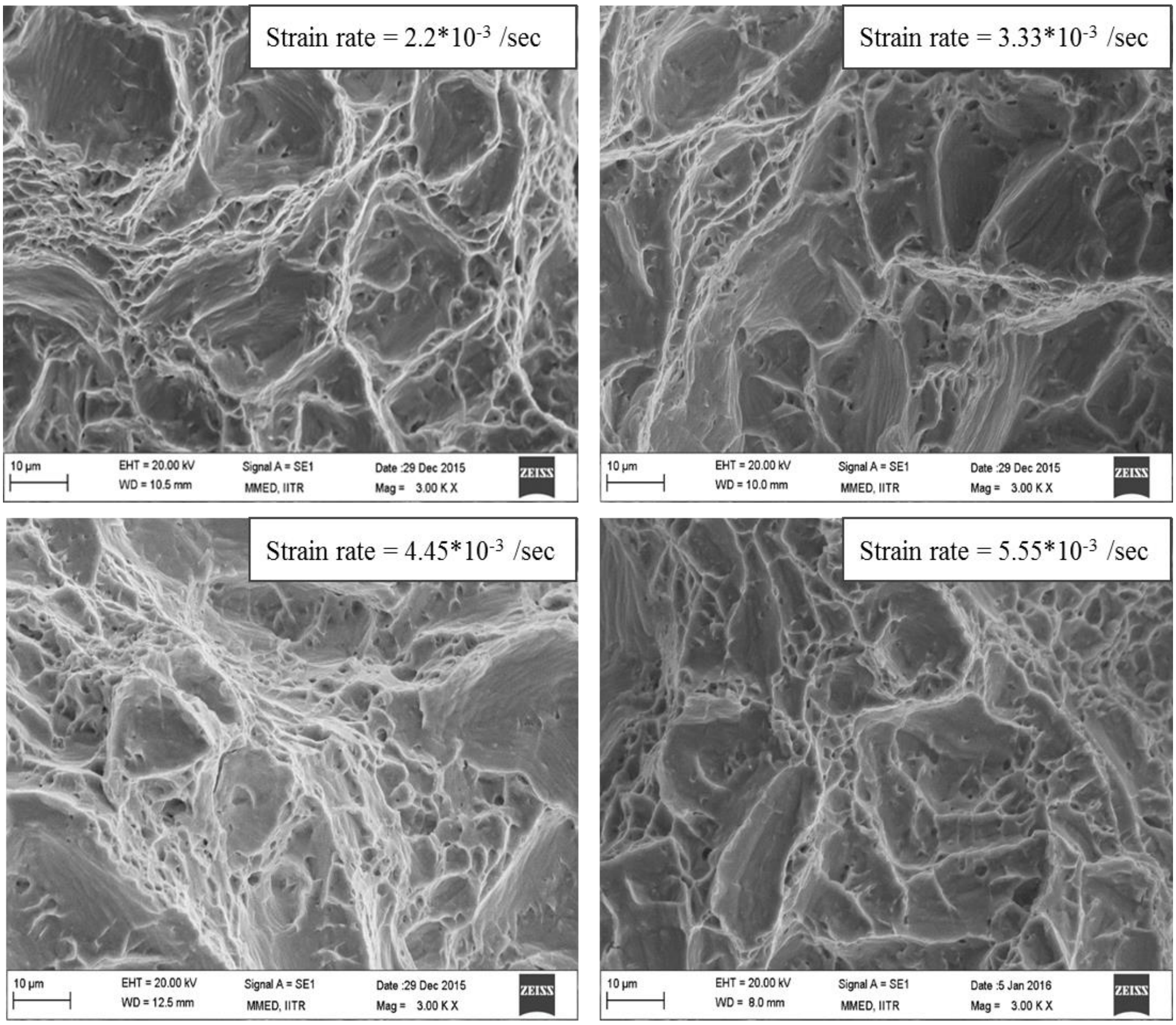

Figure 22 SEM micrograph of the fractured surface of 21mm Annealed sample at different strain rate

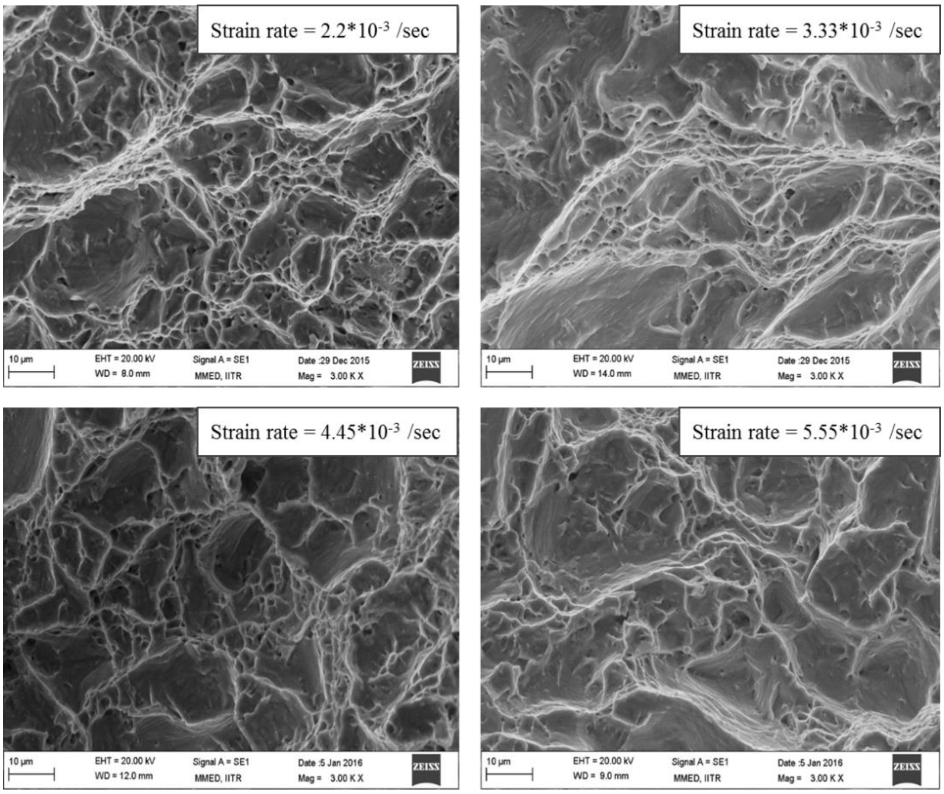

Figure 23 SEM micrograph of the fractured surface of 19mm swaged sample at different strain rate

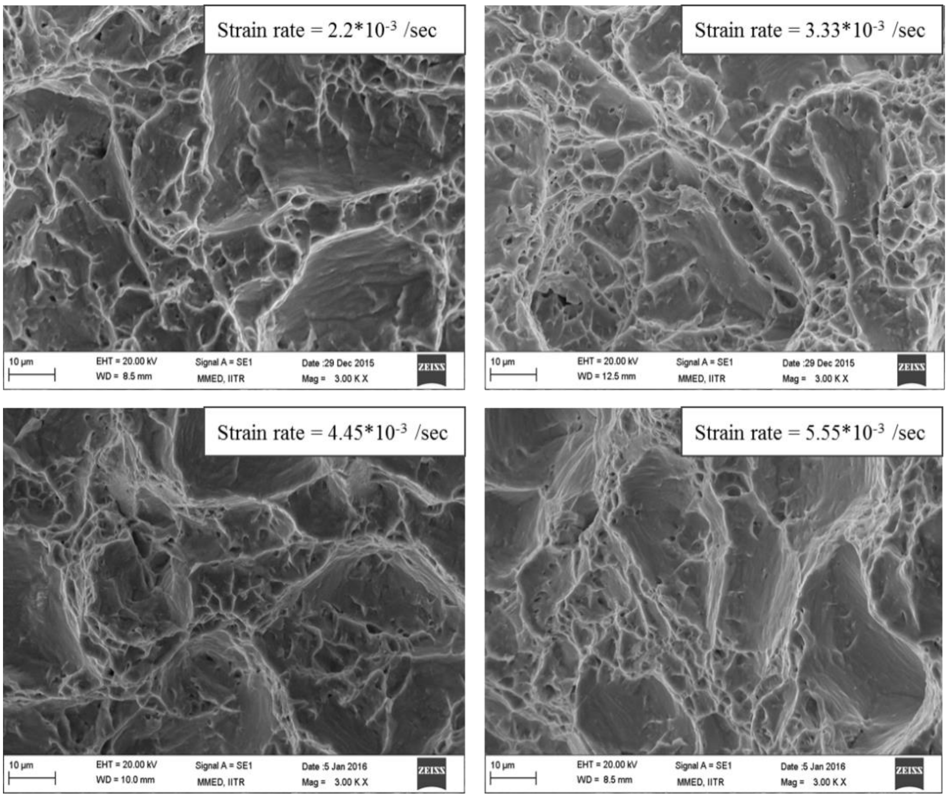

Figure 24 SEM micrograph of the fractured surface of 19mm annealed sample at different strain rate

4.4 X-Ray diffraction

Figure 25 reveals the presence of α phase in the Zircaloy 4 as all the peaks in the pattern match with the reference pattern (98-007-1958) reported for the α phase of zirconium in inorganic crystal structure database (ICSD). Intensity of the (10-10) plane is high in 23 extruded samples this mean that the grains in this sample are oriented towards (10-10) plane. (10-10) is the prismatic plane and second most highly dense plane in HCP structure. This plane helps in deformation of hcp crystal by slip. The intensity of this plane increases slightly after swaging it to 21mm diameter. After the intermediate vacuum annealing treatment at 732°C for 3 hours the grains in the alloy reorient themselves along the (11-20) plane as the intensity of the peak of that is plane is higher.

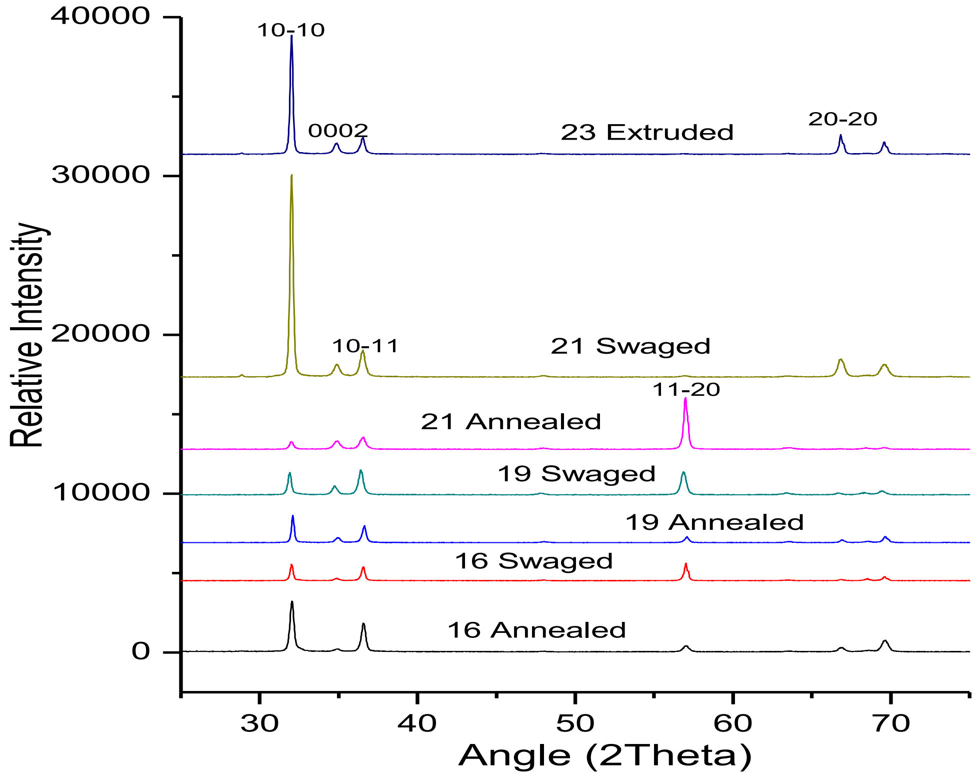

Figure 25 XRD plot between relative intensities and 2theta of Zr4 alloy at different conditions.

16 mm swaged sample shows the presence of both plane in almost equal percentage i.e. the presence of prismatic and pyramidal plane (11-20). After the completion of all the stages in swaging the final annealed sample i.e. 16 mm Annealed sample shows the intensity of the prismatic plane is high.

This study reveals the anisotropic behaviour of Zircaloy during the deformation and the evolution of the texture. This study is further validate by EBSD analysis. Figure 26 reveals the peak broadening in the Zircaloy4 samples with the highest broadening in the 21 mm swaged samples. It has been reported that peak broadening occur due to the presence of large number of defects i.e. the dislocation density must be higher than the $5*10^{12}$ /m^2. [24]

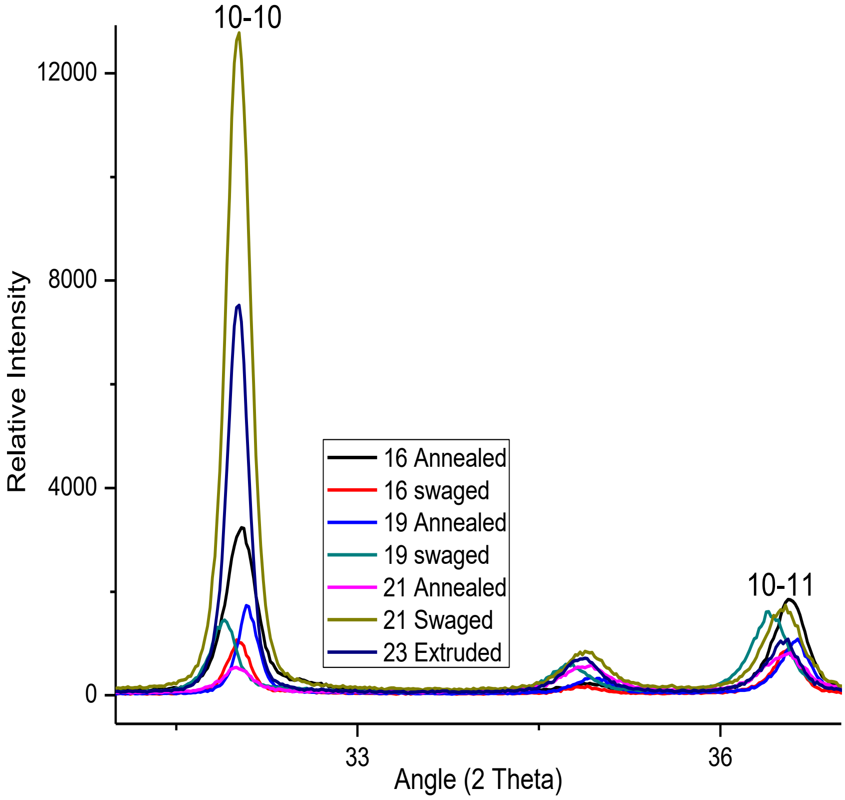

Figure 26 XRD peaks of Zr4 sample at different condition. Showing the effect of swaging on peak broadening

The dislocation density determines was found out to be $3.52*10^{15}$/m^2 for 23 extruded it increases slightly to $3.83*10^{15}$/m^2 for 21 swaged and then decreases to $4.714*10^{13}$/m^2 for 21 Annealed again increases to $1.64*10^{15}$/m^2 for 19 swaged and decreases to $2.612*10^{14}$/m^2 . The dislocation densities for 16 swaged and annealed samples are $9.8*10^{14}$/m^2 and $3.45*10^{14}$/m^2. The trend is same as was for tensile strength and hardness i.e. the dislocation density is decreases continuously from its previously swaged sample and increases continuously from its previously annealed sample.

Table 5 Values of dislocation density determined using Hall Williamson technique of Zr4 samples at different conditions.

Samples	23 extruded	21 swaged	21 annealed	19 swaged	19 annealed	16 swaged	16 annealed
Dislocation Density (/m2)	$4.52*10^{14}$	$2.83*10^{15}$	$3.714*10^{13}$	$1.64*10^{15}$	$4.612*10^{14}$	$9.8*10^{14}$	$7.45*10^{14}$

4.5 EBSD Analysis

The effect of swaging and intermediate vacuum annealing at 732° C for 3 hours on the orientation of grains of Zr4 samples can be visualize from figure 27. The minimum confidence index is taken to be 0.1 so that the scanning points having very low confidence index can be seen as black. EBSD has been done along the cross section of the rod. Initially most of the grains are oriented towards (10-10) plane and the grain size was found to be 4.76µm, grains are homogeneous with low angle grain boundaries and show no twin plane.

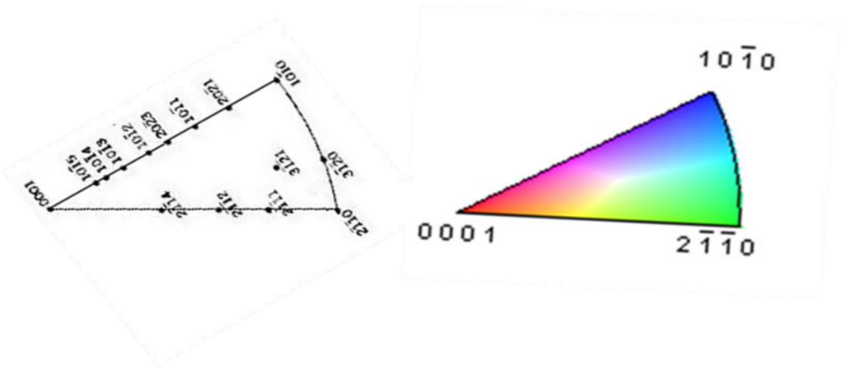

Figure 27 Inverse pole figure for Hcp material and its indexing along the boundary

After the first pass of swaging i.e. in 21 mm swaged sample the grain size is reduced to 3.55µm and deformed grains are observed. Grains get elongated due to the compression process and the orientation remains same as was in 23 extruded samples i.e. along (10-10) plane. After the annealing treatment the recrystallized grains are observed. The grains orient towards the (11-20) or (2-1-10) planes and the average grain size becomes 15.7µm with high angle grain boundries and misorientation. Annealing twins has also been observed with twinning plane of (11-26). It has been reported that at high temperature in hcp material {10-11}<10-12> twinning are observed. After swaging of 21 mm annealed Zr4 sample to 19mm diameter deformed grains are observed with compression twins {11-22}<11-23> which are indicated by the black cirles. These twins are very common in hcp material as reported in the literature. Twinning helps in deformation process by activating new slip system. After annealing treatment of 19 mm swaged sample recrystallized grains are again formed with high angle grain boundaries. The orientation of the grains were mixed. i.e. grains of the planes can be observed. Further swaging process of 19 mm annealed Zr4 sample shows the deformed grains with compression twins. The grain size plot is shown in figure 29. Increase in the grain size takes place due to several intermediate annealing steps. Effect of annealing also reveleas the evolution of texture in the material.

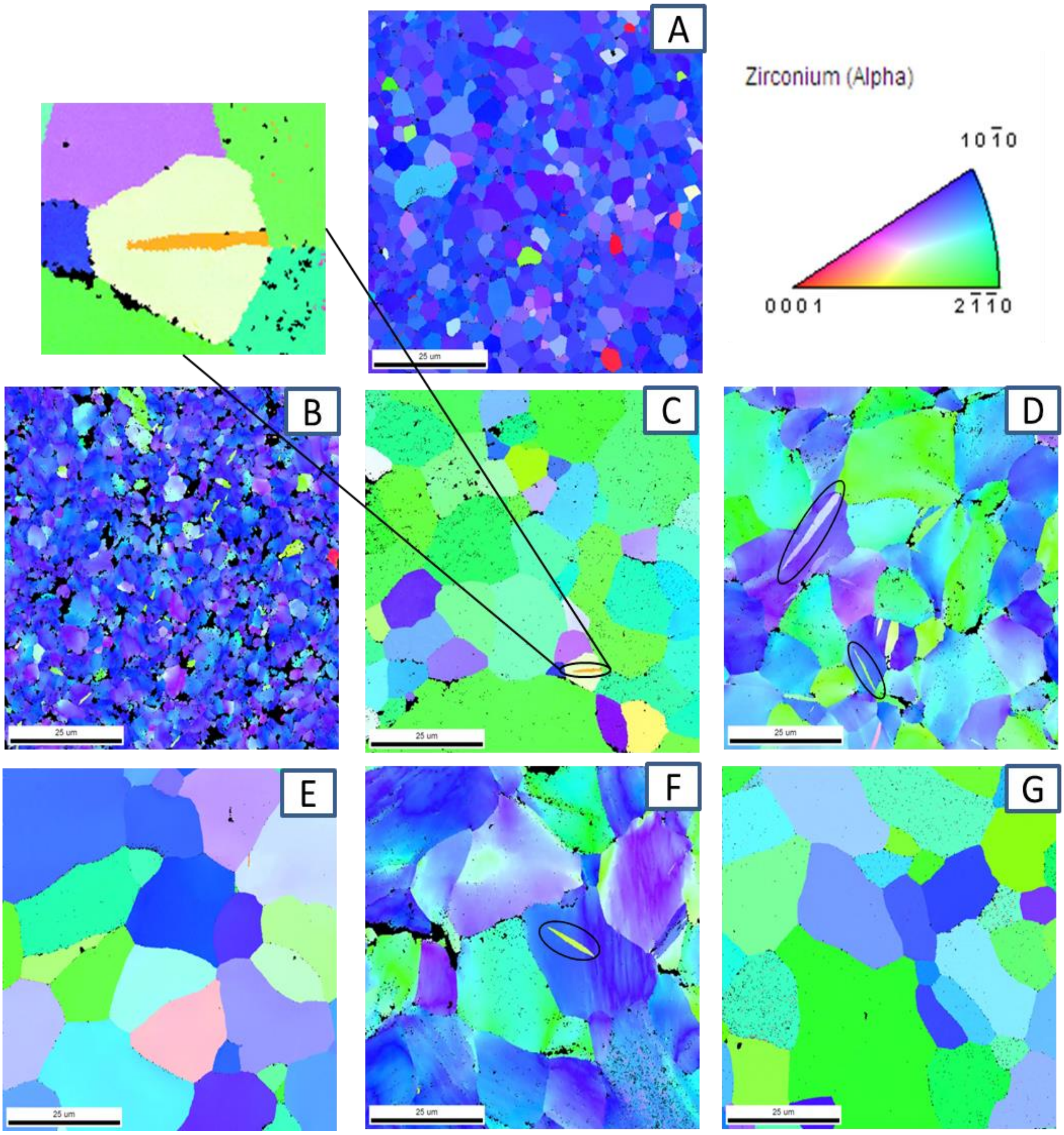

Figure 28 Inverse pole figure images of a) 23 extruded b) 21 swaged c) 21 Annealed d) 19 swaged e) 19 Annealed f)16 Swaged g) 16 annealed Zr4 samples

The average grain size determined by ebsd analysis is found to increase and was found to be almost similar as was determined by the linear intercept method. Although the sacanning area in ebsd analysis is comparetively small but the slight decrease in grains size as determined by ebsd is due to clearly visiblity of grain boundaries. Low angle grain boundaries are also clearly by ebsd analysis which is difficult to distinguish in optical microsocpy. Below is the table shows the grain size of Zr4 samples at different condition determined by linear intercept and ebsd analysis.

Table 6 Comparison of grain size by linear intercept and EBSD analysis

Samples	23 extruded	21 swaged	21 annealed	19 swaged	19 annealed	16 swaged	16 annealed
Grain size by linear intercept method	8 µm	6 µm	17 µm	14 µm	22 µm	16 µm	24 µm
Average grain size by EBSD	4.7 µm	3.5 µm	15.7 µm	13.5 µm	19.8 µm	18.9 µm	19.9 µm

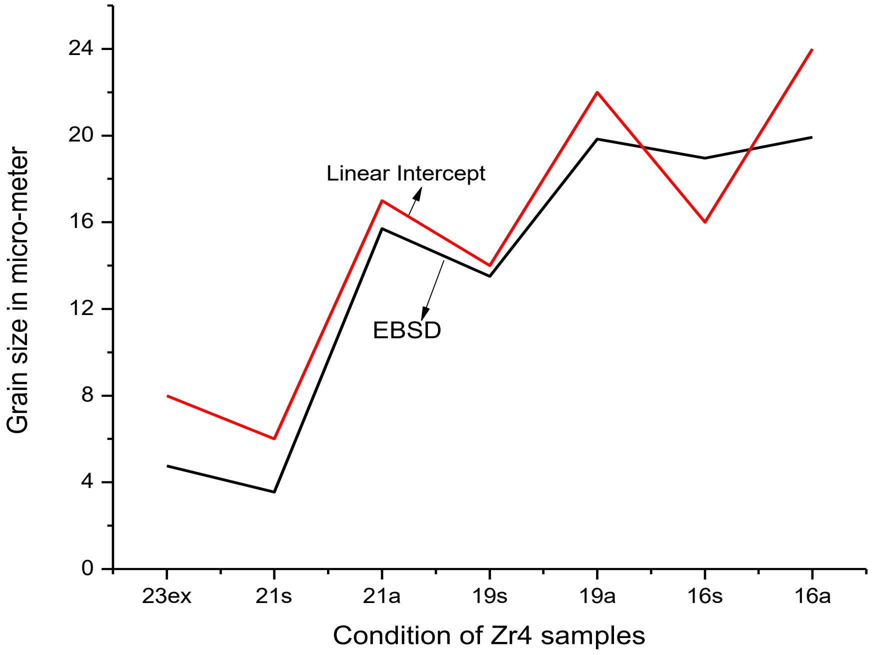

Figure 29 Grain size of Zircaloy 4 samples at different condition determined by EBSD and linear intercept method

4.5.1 Kernal Average misorientation.

Kernal average misorientation is a tool in OIM analysis software which is use to describe the localized dislocation density of the material using average misorientation value. Generally the distribution has been done in such a way that when the KAM value is greater than one than the high dislocation density is present in the material and represented by light green color in the map. If the misorientation value is greater than three then very high dislocation density is present and represented by red color. If the misorientation value is less than one then the localized dislocation are less and represented by blue color. Below is the figure of KAM maps determined by OIM analysis of all the swaged and annealed conditions.

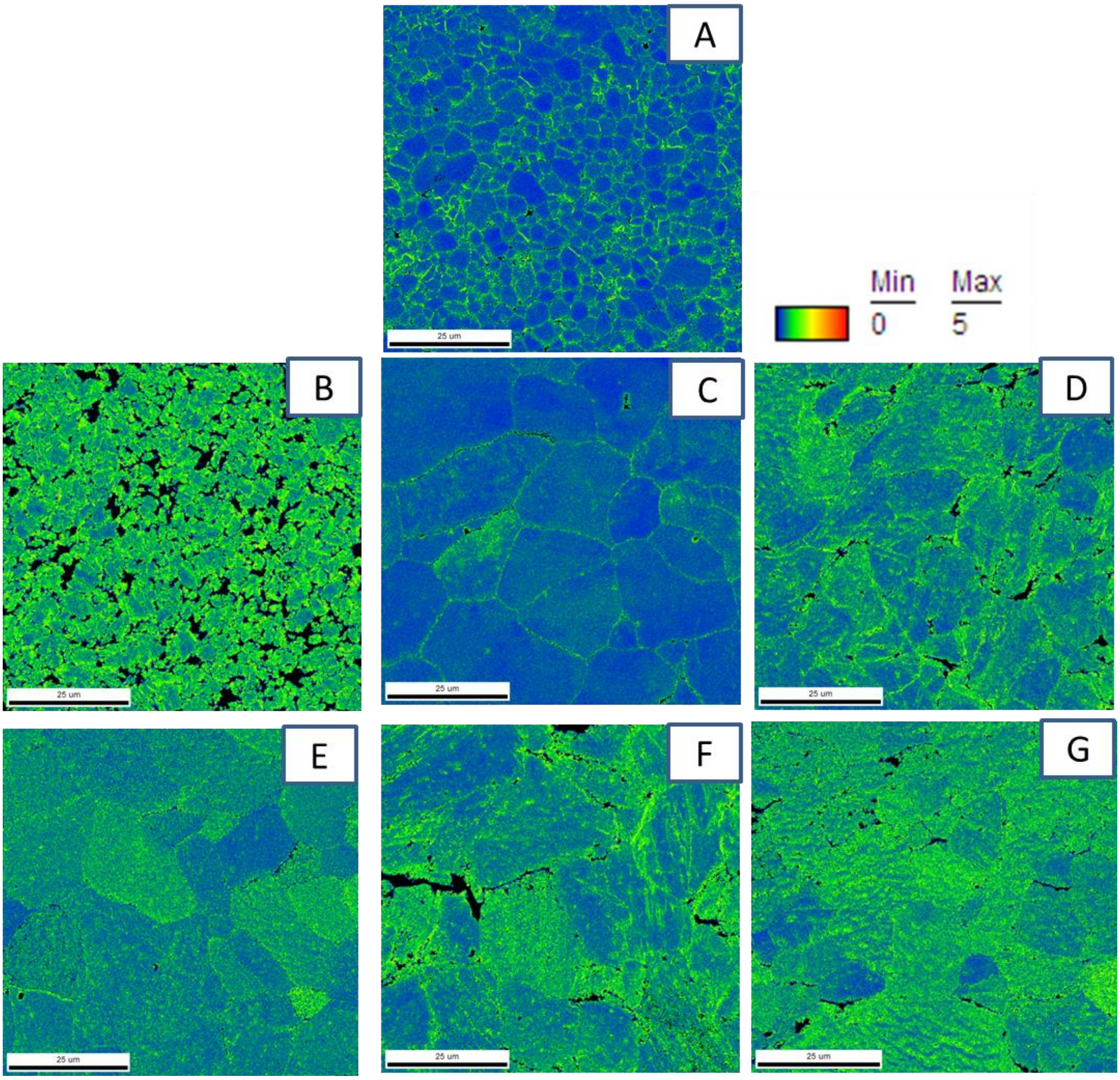

Figure 30 kernel average misorientation mapping of a) 23 extruded b) 21 swaged c) 21 Annealed d) 19 swaged e) 19 Annealed f)16 Swaged g) 16 annealed Zr4 samples

It is clear from the picture that in case of 23mm extruded sample the misorientation is generally along the grain boundary. This means the dislocation are present at grain boundary. As the swaging is performed and 23 mm extruded sample is swaged to 21 mm diameter it is clearly visible that the dislocation density is increases and has high density along the grain boundaries.

After the annealing treatment the density of dislocation decreases and gets homogenously distributed throughout the grains. The scale in the figure shows the intensity of the misorientation dark blue represent minimum misorientation while red represent maximum.

Kernal average misorientation generally signifies the amount of dislocation density and the stored energy present inside the material. It is dependent on the step size during the EBSD analysis. In the present work the step size is taken as 0.1µm. The formula for calculation dislocation density is given as [27]

$$\rho = \frac{\alpha * \theta}{b * d} \ \ldots\ldots\ldots\ldots \ (5)$$

Where α is the constant depends on the geometry of the dislocation arrangement, b is burgers vector, d is the step size and θ is the average of the Kernal average misorientation between dislocations. The value of α is 2 for tilt boundary and 4 for the twist boundary. In this work we have taken the value of α=2 because misorientation between grain boundary is not much high. The burger vector is same as was in case of XRD and θ in radians is determined by OIM software. Below is the table containing values of θ and Dislocation density per m^2 for different condition of Zr4 samples.

Table 7 KAM and dislocation density values of Zr4 samples at different conditions

Samples	23 extruded	21 swaged	21 annealed	19 swaged	19 annealed	16 swaged	16 annealed
Average KAM (θ) in radians	0.00898	0.0168	0.0143	0.0127	0.00823	0.0133	0.01193
Dislocation Density (/m2)	$6.8*10^{14}$	$1.27*10^{15}$	$1.08*10^{13}$	$9.63*10^{14}$	$6.2*10^{14}$	$1.01*10^{15}$	$9.047*10^{14}$

The values determined by this technique founds to be in good correlation with which is determined by XRD analysis using Williamson hall technique. The trend of the values is same. It increases from 23mm extruded to 21mm swaged and then decreases on annealing treatment. Finally the dislocation density becomes $9.047*10^{14}$ for 16 mm swaged sample which is determined by KAM analysis and it is found to be $3.45*10^{14}$ per meter square determined by XRD analysis.

4.6 Transmission electron microscopy (TEM) analysis

Figure 4.16 to figure 4.18 shows the TEM images of the extruded, swaged and annealed samples. The extruded sample shows recrystallized grains with dislocations inside them due to high temperature deformation process.

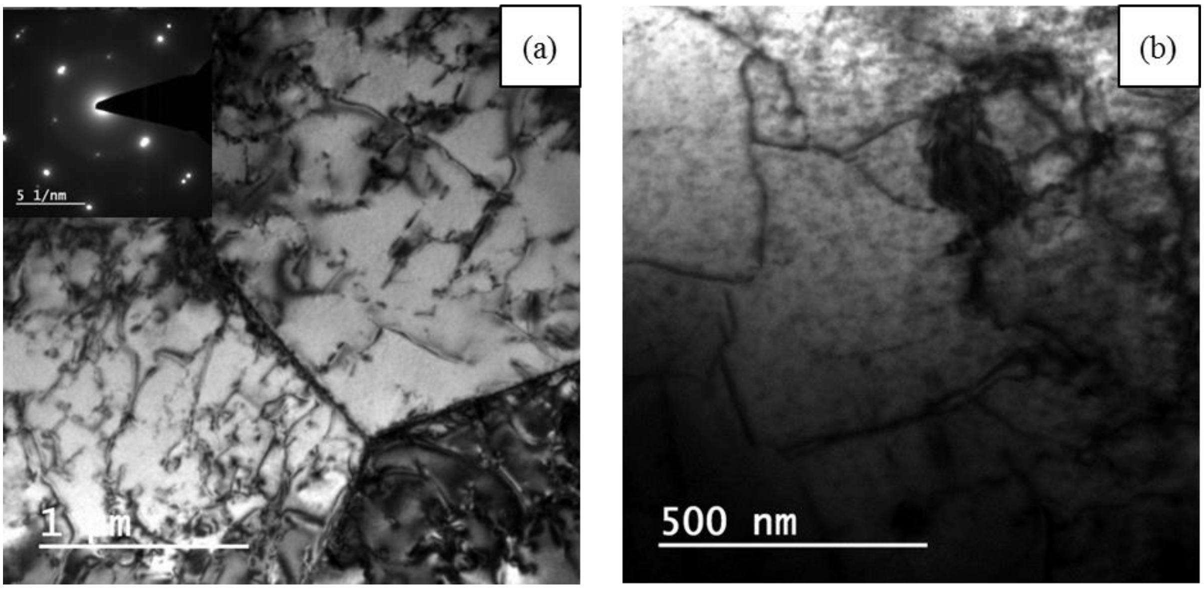

Figure 31 TEM images of 23 mm extruded sample at scale of a) 1 µm b) 500 µm and inset shows the SAD pattern

From the figure 31(a) three grains are clearly visible with the grain boundary and in figure 31(b) sevral grains are visible. The homogenous distribution of black spots in figure b shows the dislocation are homogeneously dispersed except at that black patch which is showing the accumulation of dislocation in form of dislocation cells. SAD patterns also representing the presence of grains of different orientaiton.

Figure 32 shows the TEM images of the swaged samples. The dislocation present in the swaged samples are mainly in the form of dislocation tangles. These dislocation tangles which is reperesnted by single headed arrow are formed due to the interaction of dislocation cells. It is evident that as the deforamation increase the dislocation cells are converted into dislocation tangles. The dislocation tangles are formed during initial deformation but due to dynamic recovery the tangles are slowly changing to cell structure shown as dark region in figure 32 (c). Compression twinning which is represented by double headed arrow is also observed in TEM micrograph. Twinning helps in deformation process by activating new slip system and by orienting the crystal in favourable slip direction. The compression twinning is common in HCP material due to less number of slip system. In figure 32(a) cell block structure is also visible indicated by the black circle and a deformed grain which is repressented by triangle. It can be seen that the dislocation tangles are much denser in 21 mm swaged sample. And the density of theses tangles is decreasing in 19 swaged sample. This is because 21 mm swaged sample is the most deformed structure because it is deformed directly after extrusion process. No annealing is provided between the process. In 16 mm swaged samples only dislocation cells are visible. This study shows the dislocation density is decreasing as we process the sample from 21 mm swaged to 16 mm swaged . This has already been established by dislocation density measurement by willamson hall technique in XRD analysis.

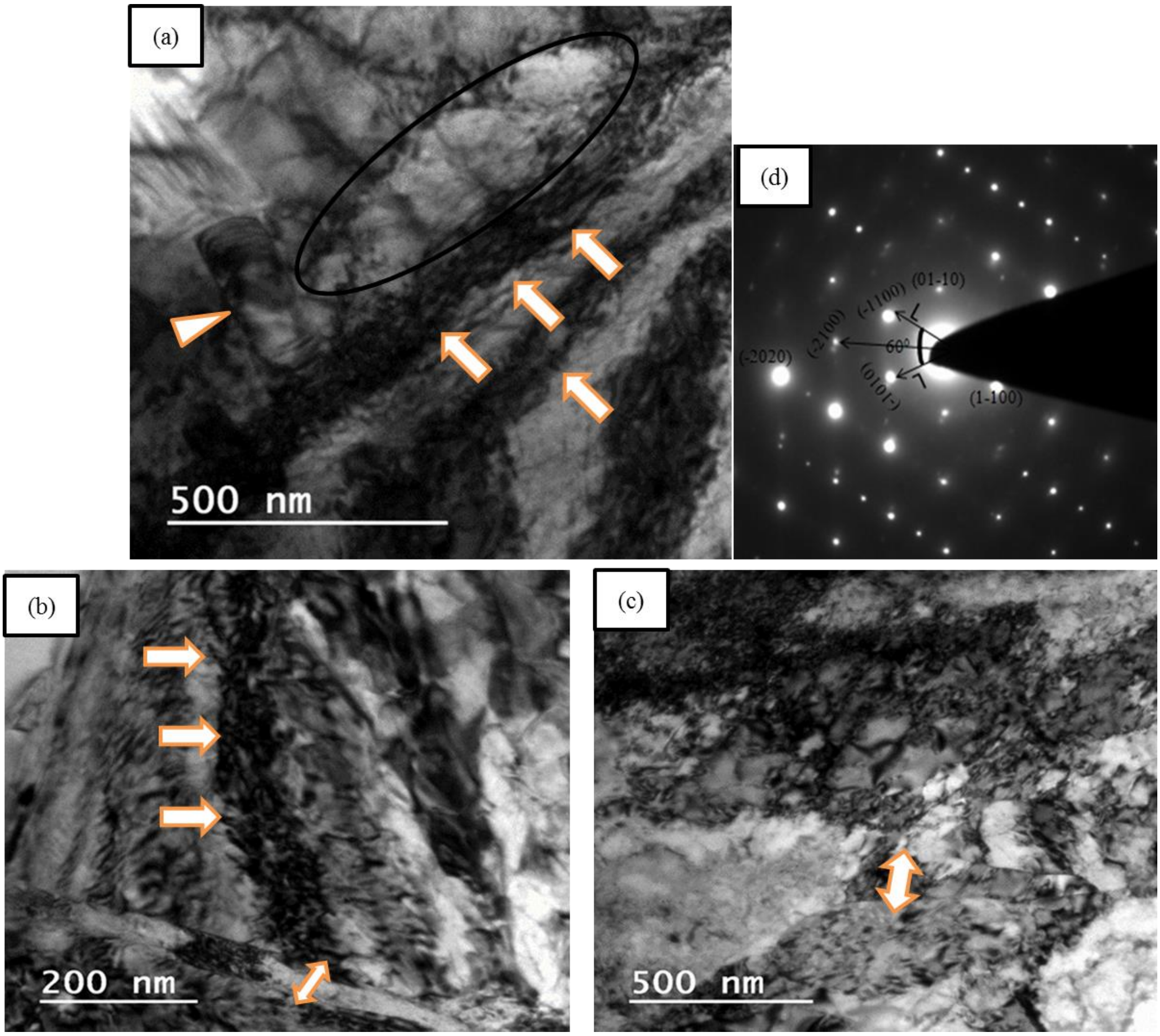

Figure 32 TEM images of (a) 21 mm swaged (b) 19 mm swaged (c) 16 mm swaged Zr4 samples (d) SAD pattern of swaged sample.

Figure 33 shows the TEM images of all the annealed Zr4 samples. It is clearly visible that the dislocation density is less and dislocation are mostly present in the form of dislocation cells. Figure 4.18(a) is repersenting the dislocation cell structure inside the grains. The grains are not visible in these micrograph because the grain size is much higher in comparison to the scale of these images. Thus the visible features are inside of a grain. Figure 4.18(b) is showing the accumulation of dislocations at the grain boundary. While in figure 4.18(c) the least dislocation density is visible in form of dislocation cells. Diconitinous arc shown in the SAD pattern of the annealed smaple also confirms the presence of dislocation cells.

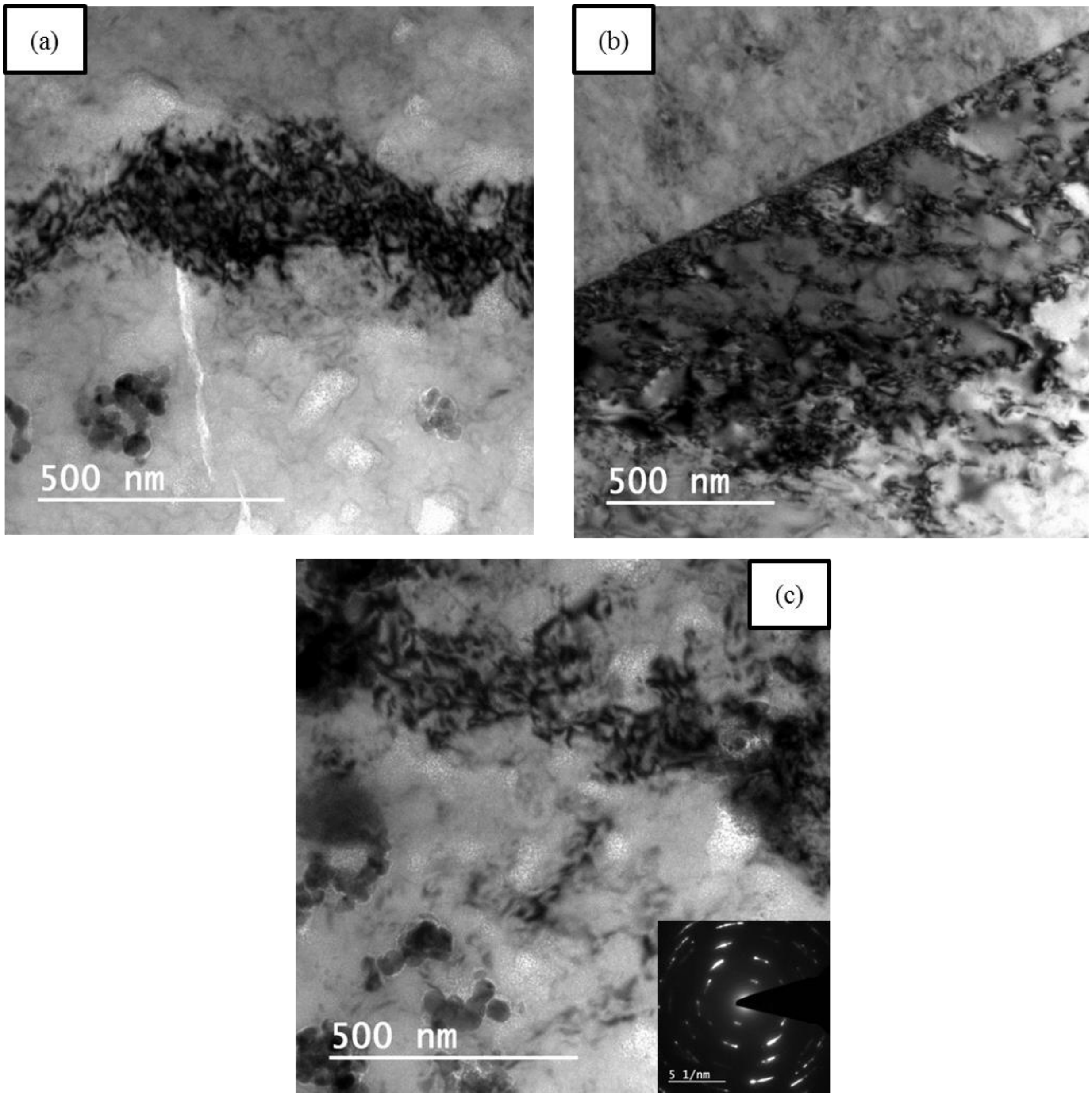

Figure 33 TEM images of (a) 21 mm Annealed (b) 19 mm annealed and (c) 16 mm annealed Zr4 sample

4.7 Corrosion test

Figure 4.19 shows the polarization curves of swaged and annealed samples of all seven conditions discussed above. The test has been conducted in 1M NaCl solution at 20°C. Corrosion rate is found to be decreasing as the swaging and annealing progressed. Corrosion rate is usually dependent on the metallurgical parameters such as grain size, dislocation density, precipitates and crystallographic texture. Generally as the grain size increases corrosion rate decreases.

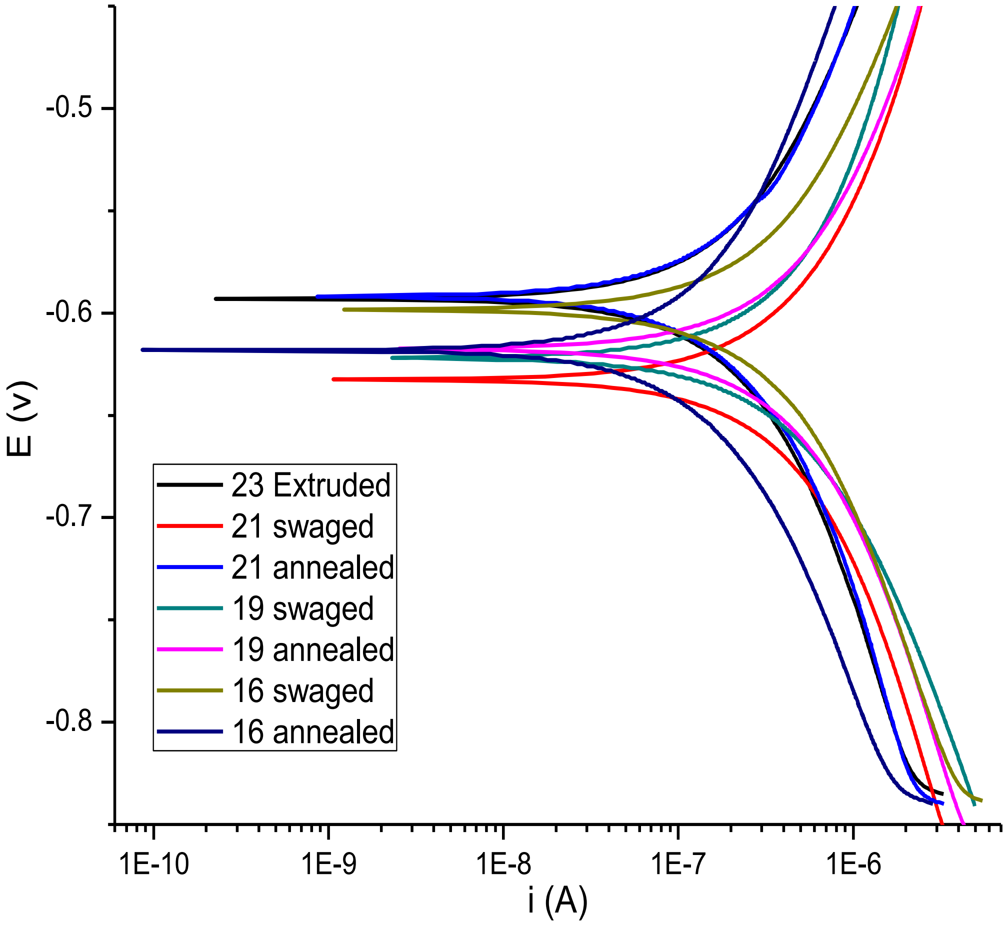

Figure 34 Tafel curve of the Zr4 samples at different conditions.

The above curve represents the anodic and cathodic polarization of the samples. And the meting points of both gives the open circuit potential which is used to determine the corrosion rate.

Higher the open circuit potential, higher will be the corrosion rate. Table 4.6 shows the value of corrosion rate at different swaging steps.

Table 8 Values of corrosion rate determined by I corrosion of Zr4 samples at different conditions.

	23 Extruded	21 Swaged	21 Annealed	19 swaged	19 annealed	16 swaged	16 annealed
I_{CORR} (micron A)	0.815	0.879	0.81	0.585	0.359	0.475	0.224
I_{CORR} per cm^2	1.135	1.224	1.128	0.814	0.5	0.661	0.311
E_{CORR} mv	-617	-633	-422	-598	-593	-592	-618
Corrosion Rate in mm/year	0.026	0.028	0.026	0.018	0.011	0.015	0.007
Corrosion Rate in µm/year	26.16	28.22	26	18.78	11.52	15.25	7.19

The corrosion rate is determined using the formula $C.R = \frac{3.24*10^{-3}*I_{corr}*E.W}{\rho}$ …… (1)

Which is given in ASTM standard of polarization potential.

Where E.W is equivalent weight and ρ is the density of the Zircaloy4 material which is determined by the rule of mixtures. The density and equivalent weight found out to be 6.484 g/cm^3 and 45.711 g/eq. respectively.

The corrosion rate is increases from 26.46 µm/year to 28.22 µm/year after first pass of swaging. This increase is due to increase in the dislocation density of the material and reduction in the grain size. After the first intermediate vacuum annealing treatment the corrosion rate has decreased to 15.25 µm/year and increased to 26.06µm/year in 19 swaged samples. It has been reduced to 13.51 µm/year for 16 swaged and 7.19 µm/year for 16 Annealed samples. Another reason for this changes in corrosion rate is assumed to be change in planar atomic density. Surface with lower planar atomic density shows higher corrosion rate because it is an electrochemical reaction between surface atoms and ions present in the solution. The high atomic density plane in hcp crystal are (0001), (11-20) and (10-10) with atomic densities of 1.15, 0.73 and 0.63 respectively. From the texture studies it can be seen that initially Zr4 alloys were oriented toward (10-10) plane i.e. in case of 23 extruded and 21 swaged samples and that's why the corrosion rate is higher for them because their atomic density is not high as compared to plane (11-20) which is the orientation of the 21 Annealed sample.

4.8 Fatigue Simulation

Fatigue simulation of all the swaged and annealed Zircaloy-4 sample was done using ANSYS-15.0 software. Gerber criteria is use for evaluation of the fatigue life because it includes both positive and negative mean stresses while other theory such as Goodman and Soderberg do not include both. Gerber criteria can be described by the following equation.

$$\frac{\sigma_{Alternating}}{\sigma_{Endurance\ Limit}} + \left(\frac{\sigma_{Mean}}{\sigma_{Ultimate\ strength}}\right)^2 = 1 \ldots\ldots\ldots\ldots\ldots (6)$$

"Weiming Sun" has worked on the fatigue behaviour of the Zircaloy-4 materials and the result of the fatigue were taken from his work. The simulated result of extruded sample were found to be in good agreement with the experimental data. Based on this we perform the analysis using tension test properties of all the swaged and Annealed material. The sample is made using solid works software and the dimension taken was according to ASTM standard of E606-12.

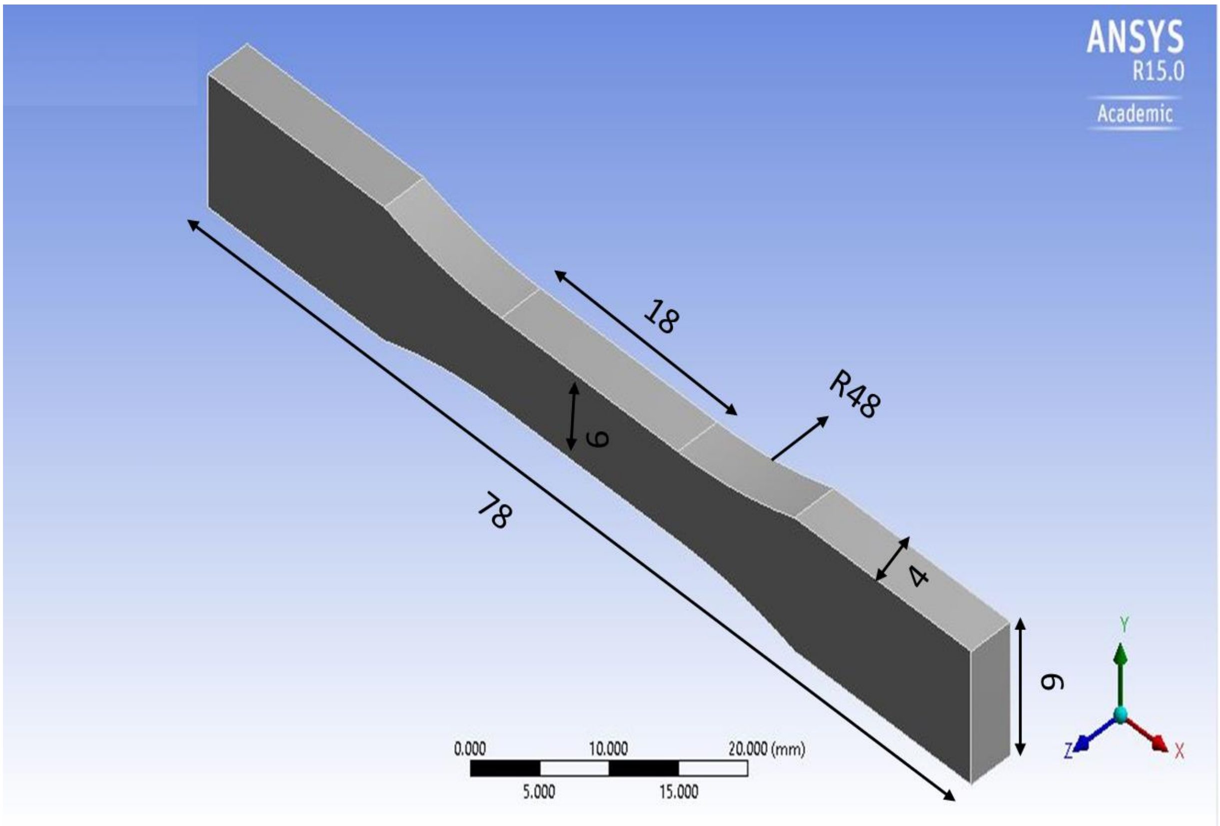

Figure 35 Fatigue sample with dimensions

"Weiming Sun" conducted his fatigue experiments on Zircaloy 4 at room temperature as well as at 380° C. He performed low cycle fatigue test on the alloy and reported the alternating stress and number of cycle data. We uses his room temperature low cyclic fatigue data and compares with our simulated data and got the almost fitting curve as shown in figure 36. After this we uses tensile properties of different swaged and annealed Zircaloy 4 material to get the simulated fatigue results at different conditions. The S-N curve of the swaged and annealed Zircaloy 4 material is shown in figure 37.

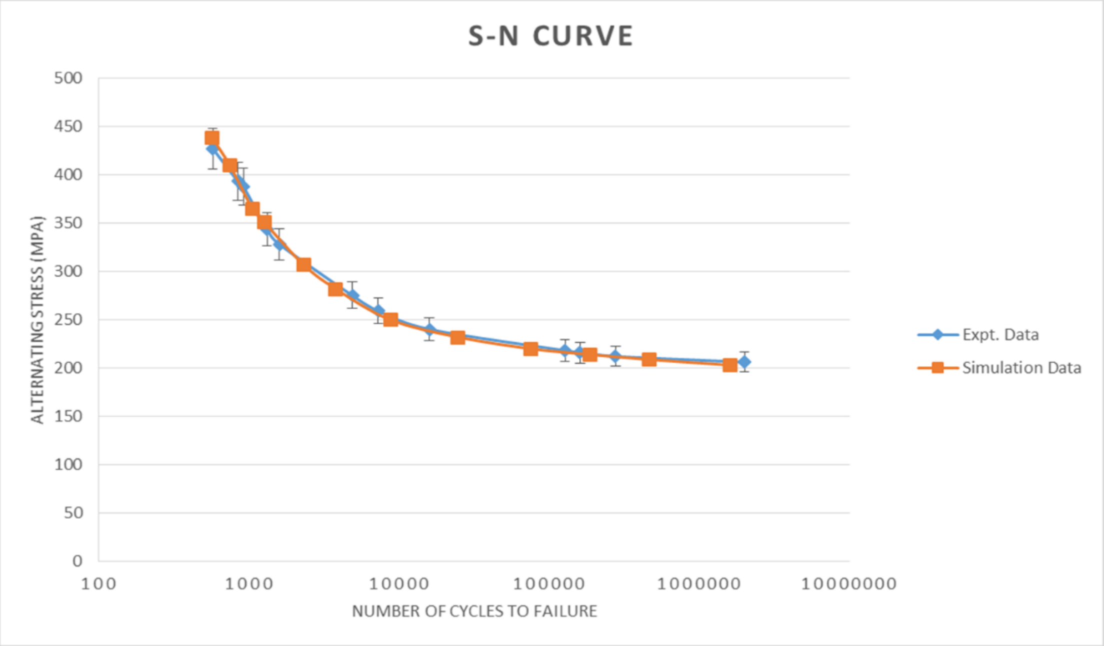

Figure 36 Comparison of fatigue result obtained with the simulated results of Extruded Zr-4 samples

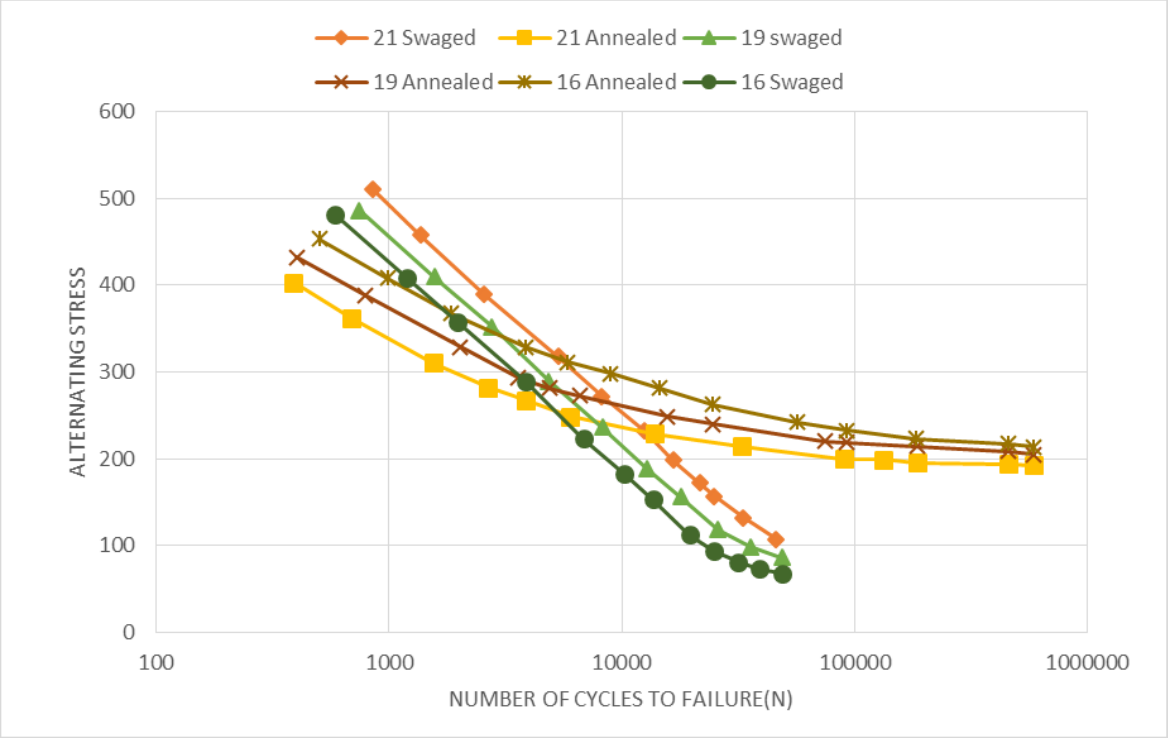

Figure 37 S-N curve of Zircaloy 4 material at different swaged and annealed condition

S-N curve obtained from the simulated result can be uses to depict that there is a steep change in the slope of the curve all swaged Zr4 samples. This is because the tensile strength of those were higher and ductility was lower. The steep slope represents the number of cycles to failure of these samples were lower i.e. the fatigue life is lower. While annealed samples shows less slope it means the material fails at higher load in less number of cycles but as we decrease the load slightly the number of cycles to failure increase to a much higher value. Of the 21, 19 and 16 mm swaged Zr4 samples 21mm swaged sample fails at higher cycle at higher load but it fails at lower number of cycle at lower loads as compared to 19 and 16 mm swaged samples. And if we compare between 21, 19 and 16 mm annealed samples then we can see that 16 mm annealed sample fails at higher number of cycle at a given load. Thus it can be depicted that 16 mm annealed sample is the best sample in terms of fatigue life. It withstands more number of cycles at higher load.

4.9 Fracture toughness Test.

Fracture toughness is a generic term which measures the material resistance to crack propagation. The behavior of any material or generally a metallic material during this test is best described by three aspects, these aspects include the fracture behavior, the strength and the deformation of the material. The material deformation behavior can be best characterized as either linear elastic, non-linear elastic or elastic plastic. As defined in ASTM E1823, the plane strain fracture toughness, K_{IC}, is the crack extension resistance under conditions of crack tip plane strain in mode-I for slow rates of loading under predominantly linear elastic conditions and negligible plastic zone adjustment. But in this study we uses ASTM E399 standard to determine the fracture toughness values. According to this standard the recommended specimens for the plane strain fracture toughness testing are three point bend SE(B) specimen, compact C(T) specimen , disk shape compact specimen, arc shape tension and arc shape bend specimen. In present study we use three point bend specimen. The standard requirement of the specimen are w=2B, H=1.2w, s=4w, L>=3w, and a/w should be around half.

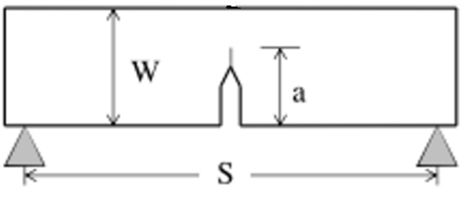

Figure 38 Three point bend specimen with dimensions.

Three point bend test is use to determine the k_Q values. Then then we try to validate these values for the fracture toughness values. The plot between force and extension is shown in figure 36 which is obtained by three point bend test. The maximum load obtained from the curve is taken as P_Q , from the P_Q value condition fracture toughness (K_Q) is calculated using equation [28][29]

$$k_Q = \frac{P_Q}{B\sqrt{W}} * f\left(\frac{a}{W}\right) \ldots\ldots\ldots (7)$$

Where B and W are the dimensions of the specimen, f(a/w) is the geometry parameter which is determined using the formula[30]

$$f\left(\frac{a}{w}\right) = \frac{3*\frac{s}{w}*\sqrt{\frac{a}{w}}}{2\left(2+2\frac{a}{w}\right)\left(1-\frac{a}{w}\right)^{\frac{3}{2}}}\left[1.99 - \frac{a}{w}\left(1-\frac{a}{w}\right)\left\{2.15 - 3.93\left(\frac{a}{w}\right) + 2.7\left(\frac{a}{w}\right)^2\right\}\right] \ldots\ldots\ldots (8)$$

The dimension used are s=64mm, B=7.5mm, w=15mm, a=7.55 mm which is following all the above criteria for the required three point bend specimen.

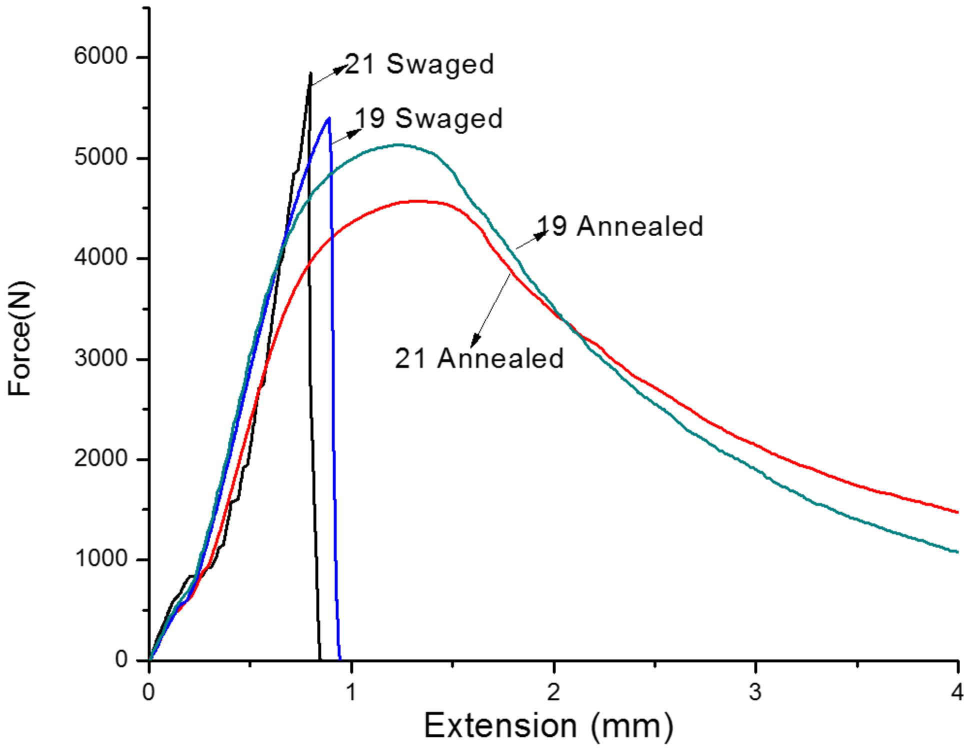

Figure 39 Force versus elongation curve of Zr4 material at different conditions

It is important to have high K_{IC} in nuclear industries because any leakage will result in leakage of the uranium fuel which was stored in the zirconium tube will comes into contact with coolant and may damage the entire reactor.

In this work a/w is taken to be 0.55 which gives the value of f (a/w) = 13.35

The values of K_Q of Zircaloy4 determined by above formula is given in table 9

Table 9 values of KQ for Zr4 samples at different conditions

Samples	21 swaged	21 annealed	19 swaged	19 annealed
K_Q MPa(m)$^{0.5}$	84.8	66.41	78.38	74.55

The specimen size imposed in ASTM E399 with an intention to ensure that a K_{IC} measurement corresponds to lower bound at the plane strain plateau.

For K_Q to be a valid K_{IC} the following condition must be satisfied [29]

$$B, a \geq 2.5\left(\frac{K_Q}{\sigma_{ys}}\right)^2 \ldots\ldots\ldots (9)$$

By putting the value of K_Q and yield stress values the B values comes in the range of 49.9mm to 68.9mm. This much value of B is surely impossible to get so an alternative method is adopted.

“Wallin” improves the ASTM standard E399 test method by determining K_Q at a fixed amount of crack growth like 0.5mm or 2% ligament of the 1T size to eliminate the size effect. In addition, “Joyce and Smudz” demonstrated that the J-integral determination can be used to evaluate K near crack initiation (denoted K_{JC}) in an accurate and size insensitive fashion and thus a recent ASTM standard E1820-11 provides an alternative test method that permits valid fracture toughness estimation through invalid K_{IC} test.

According to this standard K_{JC} is determined as [29]

$$K_{JC} = \sqrt{\frac{E\,J_C}{(1-\upsilon^2)}} \ldots\ldots\ldots\ldots (10)$$

Where E is the young’s modulus of the material, υ is the possion’s ratio and J_c can be determined using the formula [29]

$$J = \left(\frac{1+\alpha}{1+\alpha^2}\right) * \frac{2A_{tot}}{Bb} \text{ .... } (11)$$

Where A_{tot} total area under load displacement curve, and b=w-a; where alpha is parameter which is define as [29]

$$\alpha = 2\sqrt{(\frac{a}{b})^2 + \frac{a}{b} + \frac{1}{2}} - 2(\frac{a}{b} + \frac{1}{2}) \text{ .... } (12)$$

The table 10 comprises the values of J_c and K_{JC} which is determined using above formulas

Table 10 Values of JC and KJC of the zircaloy4 samples at different conditions

Samples	21 swaged	21 annealed	19 swaged	19 annealed
P_Q max. load (N)	5880	4570	5393	5130
Area under P_Q (J)	2.35	3.84	2.23	4.08
K_Q MPa(m)$^{0.5}$	84.8	66.41	78.38	74.55
J_C (KJ/m^2)	98.19	150.55	90.32	165.27
K_{JC} MPa(m)$^{0.5}$	114.64	128.7	101.94	139.89

The values determined by three point test is in good correlation with the reported fracture toughness values of Zircaloy4. The fracture toughness at crack initiation point for 21 swaged Zircaloy 4 is 114.64 MPa√m and its value increase to 128.7 MPa√m after vacuum annealing treatment.

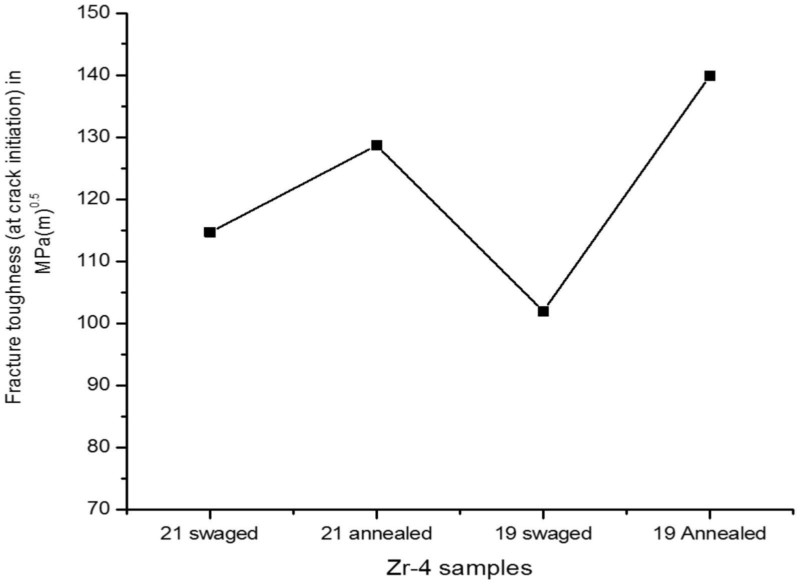

Figure 40 Variation of fracture toughness at crack initiation (K_{JC}) at different Zircaloy4 samples

The reason for this increase in value is the increase of the plastic zone at the crack tip and causing crack blunting and preventing crack propagation. After swaging of 21 mm annealed rod to 19 mm diameter value of fracture toughness at crack initiation drops down to 101.94 MPa√m. The reason is opposite of the above i.e. low plastic zone formation at the crack tip and sudden failure takes place. The value of fracture toughness at crack initiation is increased to 139.89 MPa√m after the vacuum annealing treatment of the 19mm swaged rod. This value is higher as compared to 21 mm annealed sample and it’s a good indication as the higher toughness values means higher crack resistance form growth.

Conclusions

The tensile and hardness test was carried out on Zircaloy 4 samples which are cold worked by the process known as swaging or rotary forging. The tensile test shows significant improvement in the yield strength of the samples with the loss of ductility and toughness. Ductility and toughness is restored by the annealing of the alloy at 732°C for 3 hours in Vacuum. The XRD analysis on the alloy was done at different step in the complete swaging process which is used to measure the dislocation density in the alloy after every step. Amount of dislocation density increases significantly after swaging as expected and shows a good correlation with the hardness values. From Microstructural features obtain via optical microscopy grain size is determined via linear intercept method and validated by EBSD analysis. EBSD also helps in understanding the evolution of the texture in the material by IPF image. And the values of dislocation density is validated by Kernal average misorientation dislocation density measurement method. TEM images shows the dislocations presents in the alloy after and before the swaging process and also after the annealing treatment. TEM images of the extruded sample shows that the dislocation density is high and it is in the form of cells which is spread on the maximum area of the sample. TEM observation of the swaged samples shows that as the deformation increases, the formation of dislocation cells and dislocation tangles occurs. It is evident that after annealing the dislocation density has been reduced and dislocations presents is in the form of cells. Corrosion rate is found to be decrease after intermediate annealing treatment and its value is lowest for 16mm annealed sample which is the final product for the end plug. Values of fracture toughness is also be in good correlation with those reported in the literature and it is found to be increasing first with the swaging process, value of fracture toughness for 16 mm annealed sample is higher than 19 mm annealed sample which is beneficial. All the above study suggest that the reduction of 23mm diameter rod to 16 mm diameter rod via several steps is beneficial to improve its mechanical and microstructural properties.

Scope for the future work

In present work characterization was done on the surface perpendicular to the axial direction i.e. along the cross section of the rod, a study characterization study can be done along the radial direction of the rod to visualize better the effect of swaging on the grain size and the orientation. Residual stress analysis can also be done to determine the internal stress generated after the swaging process and to optimize that how much residual stresses are left after the annealing treatment. Experimental fatigue analysis can also be conducted to check that the results obtained via simulations are in good agreement with the experimental or not. Non-destructive testing technique will help in determining whether there are any internal voids or crack generated after the swaging process or not. And finally other SPD processes like ARB, Forging can be done on the swaging to further enhancement in the properties

References

[1] W. Harlow, H. Ghassemi, and M. L. Taheri, “Determination of the initial oxidation behavior of Zircaloy-4 by in-situ TEM,” *J. Nucl. Mater.*, vol. 474, pp. 126–133, 2016.

[2] K. L. Murty and I. Charit, “Texture development and anisotropic deformation of zircaloys,” *Prog. Nucl. Energy*, vol. 48, no. 4, pp. 325–359, 2006.

[3] C. National, D. E. Atbmica, and B. Aires, “Tensile properties of Zircaloy-4.pdf,” vol. 67, pp. 198–206, 1977.

[4] C. L. Withmarsh, “Review of Zircalloy-2 and Zircaloy-4 Properties Relevant to N.S. Savannah Reactor Design,” *(No. ORNL-3281). Oak Ridge Natl. Lab., Tenn..*, vol. 4500, 1962.

[5] S. Goel, N. Keskar, R. Jayaganthan, I. V. Singh, D. Srivastava, G. K. Dey, and N. Saibaba, “Mechanical behaviour and microstructural characterizations of ultrafine grained Zircaloy-2 processed by cryorolling,” *Mater. Sci. Eng. A*, vol. 603, pp. 23–29, 2014.

[6] A. Ghaei, A. Karimi Taheri, and M. R. Movahhedy, “A new upper bound solution for analysis of the radial forging process,” *Int. J. Mech. Sci.*, vol. 48, no. 11, pp. 1264–1272, 2006.

[7] X. Han and L. Hua, “Comparison between cold rotary forging and conventional forging,” *J. Mech. Sci. Technol.*, vol. 23, no. 10, pp. 2668–2678, 2009.

[8] Kim fung, zin chu fin, “Deformation mechanism in zr-hcp alloys .” *J. Mech. sci. Technol*., vol.28, no. 24, pp. 1254-1265,2010.

[9] D. FULORIA, S. GOEL, R. JAYAGANTHAN, D. SRIVASTAVA, G. K. DEY, and N. SAIBABA, “Mechanical properties and microstructural evolution of ultrafine grained zircaloy-4 processed through multiaxial forging at cryogenic temperature,” *Trans. Nonferrous Met. Soc. China*, vol. 25, no. 7, pp. 2221–2229, 2015.

[10] M. S. Problems, “Method to determine the strain-rate sensitivity of a superplastic material from the initial slopes of its stress – strain curves,” vol. 3, pp. 1099–1103, 1998.

[11] ATI Wah Chang, “Reactor Grade Zirconium Alloys - Data Sheet,” no. 888, pp. 1–4, 2003.

[12] M. Guerain, C. Duriez, J. L. Grosseau-Poussard, and M. Mermoux, “Review of stress fields in Zirconium alloys corrosion scales,” *Corros. Sci.*, vol. 95, pp. 11–21, 2015.

[13] R. W. L. Fong, “Anisotropy factors from texture and mechanical strain in Zircaloy-4 fuel sheaths,” *J. Nucl. Mater.*, vol. 440, no. 1–3, pp. 288–297, 2013.

[14] Y. Perlovich, M. Isaenkova, V. Fesenko, O. Krymskaya, M. Lenskiy, and A. Zavodchikov, “Texture Formation in α-Zr of Zr-1%Nb Alloy under Radial Forging,” *Mater. Sci. Forum*, vol. 702–703, no. 1, pp. 842–845, 2011.

[15] Y. Wu and X. Dong, “Upper bound analysis of forging penetration in a radial forging process,” *Int. J. Mech. Sci.*, vol. 103, pp. 1–8, 2015.

[16] Y. Wu and X. Dong, “Upper bound analysis of forging penetration in a radial forging process,” *Int. J. Mech. Sci.*, vol. 103, pp. 1–8, 2015.

[17] Y. Wu, X. Dong, and Q. Yu, “An upper bound solution of axial metal flow in cold radial forging process of rods,” *Int. J. Mech. Sci.*, vol. 85, pp. 120–129, 2014.

[18] I. Alvarez-Armas and S. Hereñú, “Influence of dynamic strain aging on the dislocation structure

developed in Zircaloy-4 during low-cycle fatigue," *J. Nucl. Mater.*, vol. 334, no. 2–3, pp. 180–188, 2004.

[19] A. F. Armas, S. Hereñú, R. Bolmaro, and I. Alvarez-Armas, "Cyclic softening mechanisms of Zircaloy-4," *J. Nucl. Mater.*, vol. 326, no. 2–3, pp. 195–200, 2004.

[20] D. Twining, " Deformation Twining in Zr : Role of Orientation and Composition," J. Mater. Trasns., vol. 45, pp. 90–111.

[21] D. Ciurchea, A. V. Pop, C. Gheorghiu, I. Furtună, M. Todică, A. Dinu, and M. Roth, "Texture, morphology and deformation mechanisms in β-transformed Zircaloy-4," *J. Nucl. Mater.*, vol. 231, no. 1–2, pp. 83–91, 1996.

[22] Y. Choi and H. Inoue, "Crystallographic Texture Development and Its Effect on Corrosion Behavior of Pilgered Zirconium Alloy Tubes," *Mater. Trans.*, vol. 51, no. 4, pp. 652–658, 2010.

[23] ASTM Int., "Standard Test Methods for Tension Testing of Metallic Materials 1," *Astm*, no. C, pp. 1–27, 2009.

[24] Y. T. Prabhu and K. V. Rao, "X-Ray Analysis by Williamson-Hall and Size-Strain Plot Methods of ZnO Nanoparticles with Fuel Variation," *World J. Nano Sci. Eng.*, vol. 4, no. March, pp. 21–28, 2014.

[25] A. G.-97 (2014), "Standard test method for conducting potentiodynamic polarization resistance measurements," vol. 97, no. Reapproved, pp. 1–4, 2014.

[26] T. Kunimine, N. Takata, N. Tsuji, T. Fujii, M. Kato, and S. Onaka, "Temperature and Strain Rate Dependence of Flow Stress in Severely Deformed Copper by Accumulative Roll Bonding," *Mater. Trans.*, vol. 50, no. 1, pp. 64–69, 2009.

[27] C. Moussa, M. Bernacki, R. Besnard, and N. Bozzolo, "About quantitative EBSD analysis of deformation and recovery substructures in pure Tantalum," *IOP Conf. Ser. Mater. Sci. Eng.*, vol. 89, no. 1, p. 012038, 2015.

[28] X. K. Zhu and J. A. Joyce, "Review of fracture toughness (G, K, J, CTOD, CTOA) testing and standardization," *Eng. Fract. Mech.*, vol. 85, pp. 1–46, 2012.

[29] W. Conshohocken, "Standard Test Method for Measurement of Fracture Toughness 1," no. April 2000, pp. 1–56, 2001.

[30] ASTM Stadard E-399, "Standard test method for plane-strain fracture toughness of metallic materials," *Annual Book of ASTM Standards*. p. 422, 1999.